Improving Solid State Batteries Using Bio-derived Alginates

Ashwin Vijay

TU Delft

Improving Solid State Batteries Using Bio-derived Alginates

by

Ashwin Vijay

to obtain the degree of Master of Science in the field of Sustainable Energy Technology

at the Delft University of Technology.

to be defended publicly on Monday September 30, 2019 at 09:30 AM.

Student number:	4741420	
Project duration:	January 2nd, 2019 – September 30th, 2019	
Thesis committee:	Dr. E. M. Kelder,	TU Delft, supervisor
	Prof. dr. S. J. Picken,	TU Delft,
	Dr. S. W. H. Eijt,	TU Delft,
	Dr. S. Basak,	TU Delft, daily supervisor

This thesis is confidential and cannot be made public until December 31, 2020.

TU Delft

Abstract

Advancements in energy storage technologies need to keep pace with the accelerating transition to renewable energy sources. Li metal anodes and high voltage cathode materials are widely considered to be the path into next generation Li-ion batteries, while the scare amounts of lithium in the earth's crust has prompted research into other battery materials. Of these, Sodium-ion batteries are extremely interesting due to the abundance of Na, similar insertion chemistry to Li as well as the possibility of using aqueous electrolytes due to higher redox potential. Next generation Li-ion batteries are currently held back due to issues like - dendrite formation at the metal anode which may lead to internal short circuiting and thermal runaway of the organic electrolyte. Similarly, Na-ion systems have issues with organic electrolytes due to the limited solubility of Na electrolyte salts. Solid state electrolytes (SSEs) have rapidly garnered interest as a potential alternative. SSEs vastly improve battery safety due to their superior thermal stability and mechanical strength. However, there are still limitations for SSEs in both these systems that need to be resolved prior to implementing these electrolytes in commercial batteries.

In this study, alginate salts, which are natural polysaccarides extracted from brown algae, have been examined as a solution to the problems in these systems. Initially, sodium and lithium salts (NaAlg and LiAlg) of alginic acid were synthesized followed by their physical characterization. Conductivity for sodium and lithium alginate (with 0% water) were both promising at 0.2 mS/cm. Additionally, both LiAlg and NaAlg exhibit excellent performance as binders in anode systems compared to PVdF (polyvinylidene difluoride) binders.

For utilizing the LiAlg in Li solid-state batteries, NaSICON-based LAGP electrolyte was synthesized and characterized for this study. The degradation of LAGP on Li contact has already been well researched. To combat the issue, we try to utilize a layer of LiAlg as protective layer at the LAGP surface. The coated LAGP remains stable against Li without undergoing degradation. The Li cyclability and electrochemical performance of LiAlg was further analysed by coating it on a various electrodes and studying their rate capabilities against Li. LiAlg displayed excellent performance as a secondary polymer electrolyte on the surface and in the bulk of the electrodes. These tests show exceptional cycling performances and establish a proof of concept for LiAlg as a polymer electrolyte.

NaAlg which was chosen as the electrolyte in Na-ion batteries, displays better gelation properties. The effects of water content and operating temperature on Na conductivity were investigated. For a fixed water content, increasing the temperature results in improved conductivity - though this effect is more prominent at higher water concentrations and within the margin of error at lower water concentrations. At a fixed temperature, the conductivity shows linear improvement in at low ($\leq$25%) and high ($\geq$90%) water concentrations, while remaining constant between 25% and 90%. Additionally, the performance of NaAlg electrolytes (2w% NaAlg aq. solution) and GPE (20w% NaAlg Gel Polymer Electrolyte) was compared with the conventional Na_2SO_4 electrolyte. During these tests, the electrolyte underwent degradation possibly caused due to cross-linking induced by the dissolution of Mn^{2+} from the cathode on de-sodiation. Nevertheless, as a proof of concept, the NaAlg showed promise as an electrolyte (aq. and GPE) but further system optimization needs to be done to fully establish its scope as electrolytes for Na batteries.

Acknowledgements

As I near the end of my time at the RID as a masters student, I look back at the last nine months with a sense of fulfillment and gratitude. The time I spent here during my internship and thesis have provided me with a wealth of knowledge and experience which will undoubtedly aid me in my career.

The successful completion of this thesis was a direct result of the guidance and assistance of some exceptional people and I am extremely privileged to have gotten their help over the course of the last nine months. I would like to thank Erik for his support and guidance, which was a major motivating factor for me throughout my thesis. He was always available for a quick chat, patient in answering all of my doubts and providing timely constructive feedback.

I would like to thank Shiv for sharing his expertise, and constantly extending sincere and valuable guidance and encouragement throughout the duration of the thesis. Working with him has helped me improve as a researcher. I would also like to thank Frans for his constant help, without which the experimental work would have been impossible.

I would also like all the members of the SEE research group, of which everyone helped with personal and professional advice which made the completion of this study a lot easier. Special thanks to the fellow master students, who contributed greatly to making this experience a pleasant one.

Finally, I would like to thank my family for their constant support and motivation through out this period.

Ashwin Vijay
Delft, September 2019

Contents

List of Figures

1

Introduction

1.1. The need for energy storage

The last century of industrialization has expanded the limits of science and technology to new horizons. But these advancements have resulted in adverse effects on the planet, most threatening of which is human-induced climate change. The solution to combat this global issue would be the advent of clean, economical and sustainable energy. However, as the share of renewable energy grows, so too does the problem of generation intermittency. This mismatch of energy generation and supply are caused by diurnal and seasonal fluctuations in renewable energy generators which are largely dominated by solar and wind energy. Thus, energy storage technology, especially electrochemical energy storage systems like batteries and fuel cells need to keep pace with the accelerating renewable energy transition. Since its inception in 1834, in the form of the revolutionary Daniell Cell, battery technology has come a long way, with applications ranging from the smaller scale like consumer electronics to large scale applications like electronic mobility and even grid storage [1]. These systems provide flexibility to the electricity grid by absorbing the intermittent renewable energy during peak production and provide balance to the grid during reduced supply. Nevertheless, to cope with the pace of global demand and production of energy, battery systems need to be upgraded as well to provide higher energy densities, higher capacities, increased lifetime, improved safety as well as having low cost and becoming sustainable.

1.2. Batteries

A battery is a electrochemical system (Fig. 1.1), which converts chemical energy to electrical energy through internal electrochemical reactions occurring in the electrodes (anode and cathode) and the electrolyte providing a conductive medium for the ions to move between the electrodes. Rechargeable batteries function due to the reversibility of the components and their electrochemical reactions. The functioning of a battery can be fundamentally summarised as follows:

- Discharging - During the discharging cycle, the battery functions as a galvanic cell. The anode (negative electrode) acts as the source for the ions/electrons and the cathode (positive electrode) acts as the sink. Spontaneous oxidation reactions occur at the anode/electrolyte interface, release ions into the electrolyte while the electrons are forced to travel through the circuit.
- Charging - During the charging cycle, the battery is known as a electrolytic cell. The cathode (positive electrode) acts as the source for the ions/electrons and the anode(negative electrode) acts as the sink. An external voltage is applied causing oxidation reactions occur at the cathode/electrolyte interface, which cause ion and electron flow towards the anode.

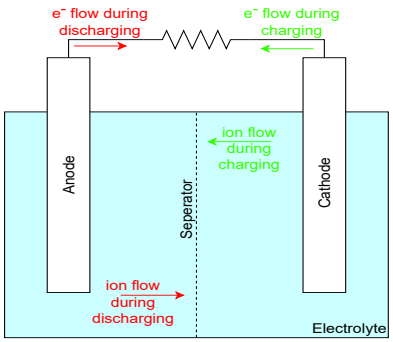

Figure 1.1: Schematic representation of a battery system and its components

1.3. Lithium-ion batteries

Lithium-ion batteries, ever since their conception in 1976 by British chemist M. Stanley Whittingham[2], have enjoyed a meteoric ascent to become the most widely utilized form of the battery. These batteries are widely used for portable consumer electronics, medical equipment, electric vehicles and are growing in popularity for military and aerospace applications. Li-ion batteries use an intercalated lithium compound as the material at the positive electrode and typically graphite at the negative electrode. Some intercalation cathode materials used utilized in current state of the art Li-ion batteries are :

- Lthium Iron Phosphate (LFP) - $LiFePO_4$[3]
  - Operating voltage of 3.4 V vs Li^+/Li.
  - Charge density of 170mAh/g.
  - High power density, long cycle life and stability at high temperatures.
  - Applications - in power tools, electric vehicles, and solar energy installations.
- Lithium Nickel Manganese Cobalt Oxide (NMC) - $LiNi_xMn_yCo_zO_2$ $(x + y + z = 1)$[3]
  - Operating voltage of 3.7 V vs Li^+/Li.
  - Charge density of 170 mAh/g.
  - High volumetric density.
  - Applications - in electrical vehicles.
- Lithium Nickel Manganese Oxide (LMNO) - $LiNi_{0.5}Mn_{1.5}O_4$[4]
  - High voltage cathode (4.9V vs Li^+/Li) with flat plateau at 4.7 V.
  - Large specific capacity of 146.6mAh/g.
  - Applications - electric vehicles, other high-power applications.

Typically, the electrolytes in Li-ion batteries consist of Li^+ salts (like $LiPF_6$, $LiBF_4$ or $LiClO_4$) in an organic solvent (such as ethylene carbonate (EC), dimethyl carbonate (DMC), and diethyl carbonate (DEC)). Typical conductivities of liquid electrolytes at room temperature are ≈10 mS/cm. At the anode side, conventional Li-ion batteries use graphite and have a theoretical capacity of about 372 mAh/g. In addition, extensive research and development to improve the anode's capacity have brought forth materials with better electrochemical properties like silicon, germanium and tin, which provide much higher capacities (are 3579 mAh/g, 1600 mAh/g, 994 mAh/g, respectively). These materials, however, suffer from mechanical pulverization caused due to high volumetric change of ≈300% caused during the lithiation and delithiation cycle [5].

1.3.1. Need for Solid-State Li-Batteries

To cope with the pace of global demand and production of energy, the battery systems need to be upgraded as well to push the boundaries of cost, energy density, power density, cycle life, and safety. Li metal anodes and high voltage cathode materials are possibly the next iterative step in next-gen Li-ion batteries. However, there arise new problems with these new step namely - dendrite formation at the metal anode which may lead to internal short circuiting and thermal runaway of the organic electrolyte caused due to higher working potentials.

Replacing these liquid organic electrolytes with solid electrolytes would physically suppress the dendrite growth. Solid state electrolytes (SSEs) also improve battery safety due to their superior mechanical, electrochemical, and thermal stability when compared to liquid electrolytes. Ideally, solid state electrolytes are required to possess the following features [6]:

- fast ion dynamics and negligible electronic conductivity (minimum ionic conductivity of $\approx 10^{-4}$ S/cm at room temperature.
- wide electrochemical potential window for battery cycling.
- exceptional mechanical strength to suppress lithium dendrite growth.
- excellent thermal stability during the cycling processes.
- simple and low cost synthetic process for large-scale production and application.

Inorganic lithium super-ionic conductors are classified into three categories: oxides, sulfides, and phosphates. Among these categories, phosphate based SSEs like the NaSICON-type materials (like LATP and LAGP) have clear advantages when compared with sulfides and oxides as they are chemically stable in air and water, exhibit excellent electrochemical stability and have low production costs and low toxicity [6]. These electrolytes with the general chemical formula $(Li_{1+x}Al^{3+}_xM^{4+}_{2-x}(PO_4)_3$, M = Ge, Ti), also possess high ionic conductivity $(10^{-4} - 10^{-3}$

S/cm). These features are very promising and have recently caused great interest in NaSICON-structured materials.

1.3.2. Challenges

Even though the outlook on NaSICON-based solid state batteries looks promising, these systems still contend with certain constraints and challenges. Some of the issues that have been identified for solid-state battery device are [7]:

1. Solid state ion diffusion -

   The physical limitations of SSEs cause slowed ion diffusion through the electrolyte bulk due to grain boundary resistances.

2. Formation of a Blocking Interface -

   The interfacial composition and structure between solid electrolytes and electrode materials usually differ from those of the bulk materials. The formation of decomposition products as in the case of Li with LAGP could inhibited the performance of solid-state devices.

3. Contact Loss on Electrochemical Cycling -

   Solid-state systems rely on ionic diffusion through the point contact of solid particles at the interface of the electrodes and electrolyte. These points experience localised mechanical stresses due to volumetric changes caused on electrochemical cycling in electrode materials, which can lead to the formation and propagation of cracks, as well as loss of contact at the interface.

1.4. Sodium Batteries

With the rapidly expanding electric vehicle industry, concerns have surfaced about the resource availability of Li and hence the future cost and feasibility of Li-ion batteries. Na-ion batteries could be a solution to this issue because of the abundance of sodium, its lower price and the similarities between Li and Na insertion chemistry. Another advantage of Na-ion batteries is the ability to include electrolyte systems due to the higher half-reaction potential for Na compared to Li. This characteristic of lower working voltages as well as the reduced solubility of Na salts in organic solvents (compared to Li electrolyte salts), could make aqueous electrolytes a viable option in Na-ion systems [8].

Research into Na-ion battery components has yield a large number of viable options. Cathodes for Na-ion system are usually phosphate based materials like $NaFePO_4$ which display high theoretical specific capacity and high thermal stability. $Na_{(0\cdot44)}MnO_2$ (NMO) has also been studied extensively due to its advantageous crystal structure forming suitable pathways for sodium conduction. Due to the suitability of the Na redox potential, various electrolytes like aqueous and solid-state systems (including gel polymer systems) have gathered great interest. These gel polymer electrolytes (GPEs) show great promise as they possess the cohesive and mechanical properties of solids and diffusive properties of liquids which makes them extremely attractive. Anodes in Na systems are usually carbon-based ones (similar to Li-ion) but these anodes are unsuitable in aqueous systems. Titanates, like $NaTi_2(PO_4)_3$ (NaTP) have emerged as water-stable Na anodes with promising performance characteristics. Even though metallic Na would be the ideal anode, its utilization has been limited due of dendrite formation and interface aging problems similar to Li-ion systems.

1.5. Scope of work

This study aims at attempting to solve some of the issues of solid-state electrolytes in both Li and Na systems by utilizing bio-derived polysaccarides called alginates (and their metal salts).

1.5.1. Scope in Li-systems

Extensive studies have already been conducted to study the effect of a passivating additional layer in Li solid state systems - this would help solve the issues of Li induced decomposition as well as improve interfacial conduction.

Wang et al. [9] studied the effect of a layer of liquid organic electrolyte (1M $LiPF_6$ in EC/DMC/DEC with a volume ratio of 1:1:1) on the surface of LATP and observed that a solid-liquid electrolyte interface was formed on the surface of the LATP. The formation of this interface served as a passivating layer which resists the continuous side reactions between LATP and Li. Another study by Yu et al. [10] performed similar trials with a gel polymer layer at the surfaces of LAGP. They reported that the introduction of a polymer layer not only protected the LAGP pellets from side reactions with lithium metal anodes but also reduced the large interfacial resistance. The physical characteristics of the polymer layer also provided relief against the mechanical stresses generated by the volumetric changes in the electrodes occurring during cycling. Meesala et al. [11] utilized a mixture of LiTFSI [Lithium bis(trifluoromethanesulfonyl)imide] and a poly(vinylidene difluoride) [PVdF] based LFP cathode slurry to form a blended cathode + polymer electrolyte coating on the surface of an LAGP pellet. They also reported good contact with the electrodes without an interfacial layer along with reasonable discharge capacity delivered against Li. However, majority of these methods utilize air-sensitive materials (the LiTFSI salt and the liquid electrolyte) and introduce further complexity to the battery manufacturing process.

Using their research as a stepping-off point, an attempt has been made to use Lithium alginate to study its feasibility in improving the problems of Li-solid state batteries. Lithium alginates are water-soluble and can be processed into layers which can be then be utilized as as a polymer electrolyte as well as a passivation mechanism. Thus, from the scope of Li systems, the research question was formulated as:

Can lithium alginate be used as a secondary electrolyte and passivating layer in Li-solid state batteries ?

1.5.2. Scope in Na-systems

As mentioned earlier, the exploration into Na-ion batteries especially aqueous Na-ion has also been gathering momentum as an alternative to combat the growing price of Li resources. Current Na GPEs are prepared by combining a polymer matrix with an ionic liquid and nanoparticles [8]. Switching to water-based GPEs would reduce the overall cost and improve the process-ability of these systems. On the other hand, sodium alginate has been extensively studied for its binding and ion-conducting properties (mentioned in Section 2.2). Thus, it would be of great interest to adapt sodium alginate into the realm of aqueous sodium-ion batteries to study the performance of a solid-state sodium-ion system. Thus, from the scope of Na systems, the research question was formulated as:

Can sodium alginate be used as an electrolyte in sodium battery systems ?

1.6. Research question and Structure of the report

The overall research question was formulated by combining the scope of work in both the Li and Na systems and was thus defined as:

Can alginate salts be utilized in constructing better solid state batteries ?

The structure of the report (and by extension - the experimental overview) is given in Fig. 1.2. First, in Chapter 2, a brief background study on alginate and their uses in batteries is discussed. Subsequently in Chapter 3, the synthesis and characterization of the different materials is explained. The different testing configurations performed during the study are also described. Proceeding to Chapter 4, initially the performance of alginates as binders is investigated. Then the different experiments carried out in the Li scope are described along with the observations and results. In Chapter 5, the results of the different experiments carried out in the Na-scope are explained. Finally, in Chapter 6, the main conclusions from this study are highlighted. The scope for these materials is vast, and thus some recommendations for future work have also been suggested.

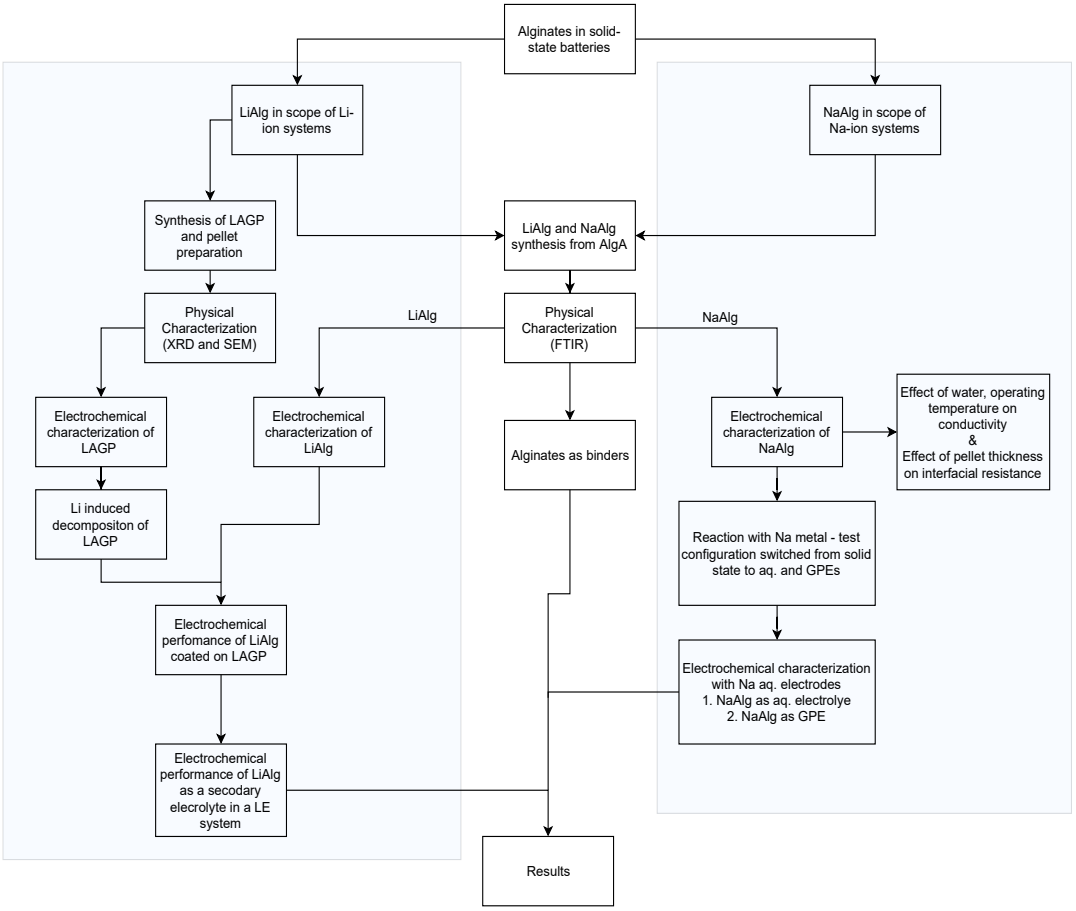

Figure 1.2: Overview of the experimental methodology and the structure of the report

2

Scientific Background

This chapter gives a brief introduction to alginic acid and the emergence of alginates into batteries in the form of aqueous binders. Some studies performed on the ion-conducting ability of sodium alginates have also been mentioned as the brief background to this study.

2.1. Alginic acid

Alginic acid is a naturally occurring polysaccharide, found in the cell walls of brown algae and aquatic micro-organisms in the form of gels (usually containing Na^{+}, Ca^{2+}, Mg^{2+} ions). These metal salts of alginic acid, known as alginates, are primarily used as a coagulator (thickening agent) in the food and biomedical industry due to their bio-compatibility, low toxicity and relatively low cost. They also exhibit excellent water absorption, which makes them useful as an additives in dehydrated products such as in the manufacture of paper and textiles.

As shown in Fig. 2.1, alginates are unbranched polysaccharides consisting of 1 → 4 linked β-D-mannuronic acid (M) and α-L-guluronic acid (G). It is comprised of sequences of M (M-blocks) and G (G-blocks) residues interspersed with MG sequences (MG-blocks) depending on the source.

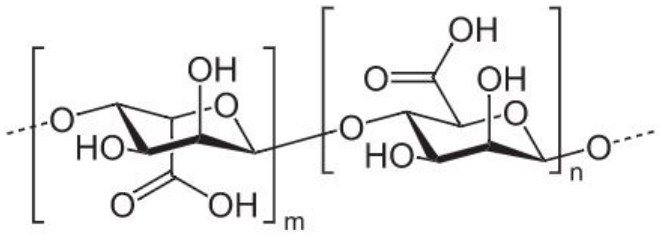

Figure 2.1: Structure of alginates with Guluronic acid block (in the left) and Mannuronic acid block (in the right).

2.2. History of alginates in batteries

The introduction of alginates and other bio-derived polymers into the battery system was done through extensive research into aqueous binders as an alternative to the conventional binders (which utilize organic solvents). Conventional research into battery materials focuses on the synthesis of the active materials with improved properties, while relatively marginal research has been devoted to the advancement of the electrically inactive components of battery electrodes, such as binders [12]. However, recent studies such as those of Bridel et al.[13] and Guy et al.[14] have shown that many important battery characteristics, including stability and irreversible capacity losses, are critically dependent on the binder's properties.

In conventional lithium-ion batteries, the electrode processing is based on the use of fluorine-containing polymers, in particular poly(vinylidene difluoride) (PVdF), as binder for the electrode preparation and toxic

N-methyl-2-pyrrolidone (NMP) as a solvent/dispersant. Switching to aqueous electrode as already achieved for graphite-based Li-ion anodes, would provide a great leap forward towards the realization of completely sustainable and environmentally friendly electrochemical energy storage devices [15].

2.2.1. Advantages of bio-derived polymers as binders

Bridel et al.[13], in their research into CMC based binders (Carboxy-Methyl Cellulose) and Magasinski et al.[16] in their work on PAA (Poly-acrylic acid) binders, showed that synthetic and bio-derived polymers that contain carboxyl groups demonstrate promising characteristics as binders for graphite and Si-based anodes. Studies by Buqa et al.[17] and Lee et al.[18] observe that by using CMC and CMC–SBR (Styrene Butadiene Rubber) binders, graphite electrodes showed lower first cycle irreversible capacity loss than PVdF-based electrodes which is attributed to faster SEI-formation induced by the interactions between the carbon and CMC.

In Si-anode systems, Lee et al.[19] reported that PAA, which contain a higher number of functional groups than CMC, adsorbs more strongly onto the anode surface via hydrogen bonding. The high availability of $-COOH$ and $-OH$ groups result in additional coordination with the active material, providing added mechanical stability to the anode [16, 20]. In addition, the polar hydrogen bonds between the carboxy groups of the binder and the SiO_2 on the Si surface would exhibit a self-healing effect and re-form if locally broken due to the volumetric expansion/contraction of Si on (de)lithiation.

The extended work conducted on CMC and polyacrylates stimulated further investigation of other functionalized binders and especially of bio-derived polymers such alginates. Polysaccarides are stable up to 200°C and thus are compatible with the relatively high electrode drying temperatures. The study by Cuesta et al.[21] showed that these bio-polymers are electrochemically inert in the potential range from 0 to 3 V vs. Li/Li^+. They are, therefore, potential alternatives to Na-CMC, providing the advantage of possessing functional groups (which instead have to be chemically introduced into cellulose). The study by Kovalenko et al.[12], showed promising results obtained using alginates as binders in Si-anode systems. Similar to CMC and PAA, alginate binders do not show swelling or a change in stiffness when in contact with the electrolyte. The study also suggests that Li^+ ion hopping may occur between neighbouring carboxylic groups, enhancing the Li+ ion conduction. Bresser et al.[15] reported that the presence of a more homogeneous distribution of functional groups in alginate (as compared to CMC), might be contributing to the improved performance. Additionally, the high polarity of the alginate chains may lead to a higher viscosity of the slurry, permitting the reduction of the total amount of binder in the electrode formulation. Similar to cross-linked polyacrylates, branched polysaccharides offer increased contact points for the binder/silicon interactions. Jeong et al.[22] observed stronger adhesion capability for charged polysaccharides which was attributed to the existence of ion–dipole interactions between –COO and the Si surface, maximized by the structure of the polymer. A recent study by Garcia et al.[23] reported higher stability and viscosity for Na-alginate slurries (of different compositions) as compared to Na-CMC. Nevertheless, although the studies are very encouraging, little is known about the process-ability, stability, and rheological properties of large-scale electrode slurries made with such bio-polymers. Understanding these properties are key factors to assess the feasibility of up-scaling the utilization of these technologies.

Solvent	Mixing	Coating	Drying
Organic liquids (eg. NMP)	Hazardous handling, requires ventilation systems and personal safety equipment	Requires controlled environments	Harmful solvent vapours, require infrastructure for collection and recovert
Water	Personal safety equipment only required for the handling of powders	Can be performed in air	No recovery necessary

Advantages of aqueous binders over conventional ones[15]

From Section 2.2.1, the advantages of aqueous binders in electrode processing over binders with organic solvents are evident. Hence, the switch from conventional binders to the use of aqueous binders would reduce the exposure of humans to these chemicals, as well as their release into the working environment. Additionally, the transition to aqueous processing is expected to have a positive impact on production costs and, in turn, on the overall battery price. Berckmans et al.[24], forecast a price of $100 per kWh for LIBs to be reached in 2030. Wood et al.[25] conducted a processing cost breakdown study, which indicated that the reduction in costs associated with the use,

drying and recovery of the organic solvent would be a key point in achieving this target. A cost comparison of binder and solvent already points to the convenience of water-based electrode processing. Presently conventional binder-solvent combinations like PVdF with a price of $8–10 per kg and NMP with $1–3 per kg (compared to about $0.015 per L for water) are a rather expensive. On the other hand, the most commonly used aqueous binders like CMC are significantly cheaper at $2–5 per kg. Even alginate salts, at about $8 per kg are a better alternative to PVdF due to the the potential cost reduction by transitioning to water-based electrode processing.

2.3. Performance of alginates as ion conducting membranes

Alginates can not only be used as binders in electrode preparation, but also as active ion conducting members in electrochemical systems like fuel cells. Mohanapriya et al.[26], in their study on proton-exchange membranes for Direct Methanol Fuel Cells (DMFCs) observed that a mixed matrix membrane based on sodium alginate displayed promising water absorption characteristics and methanol-barrier properties. Iwaki et al.[27] prepared gel polymer electrolytes (GPEs) based on sodium alginates with added salts and plasticizers. They reported that the polymer membrane displayed good ionic conductivity ($\approx 10^{-4}$ S/cm) and high thermal stability. Yamagata et al.[28] analysed non-aqueous gel electrolytes based on sodium alginate and ionic liquids for electric double layer capacitors (EDLCs) as energy storage devices. They observed that the sodium alginate gel displays high mechanical strength and excellent retention of the ionic liquid required for EDLC construction.

Majority of these studies indicate that alginate-based polymer electrolytes are excellent candidates to be used in electrochemical devices, however further investigation needs to be done into their physio-chemical properties. Limited literature is present utilizing alginates as battery electrolytes and therefore this study of their electrochemical feasibility would provide further information on their performance.

3

Materials and Methods

This chapter explains the synthesis of the different compounds used in this study. The preparation and physical characterization (visual and FTIR) of sodium and lithium alginate are discussed first. Subsequently, for the research scope of lithium alginate, the preparation of the LAGP powder and pellets is discussed followed by its physical characterization (XRD and SEM). Next, the testing configurations utilized in the study are explained like the description of the electrode preparation process, the electrochemical characterization methods and the various configurations of the alginate salts (pellets, films and electrolytes) are also briefly discussed.

3.1. Alginate Salts (Sodium and Lithium)

3.1.1. Synthesis

Required Chemicals:

The chemicals required for the preparation of preparation of sodium alginate (NaAlg) and lithium alginate (LiAlg) are mentioned below.

Chemical	Supplier	CAS
Alginic Acid [29]	Alfa Aesar	9005-32-7
Sodium Hydroxide(NaOH) [30]	Sigma Aldrich	1310-73-2
Lithium Hydroxide monohydrate($LiOH \cdot H_2O$) [31]	Sigma Aldrich	1310-66-3
Sodium Alginate [32]	Alfa Aesar	9005-38-3

Method:

Initially, NaOH and Alginic acid (AlgA) powders were mixed in 2:5 proportion in a pestle and mortar. This composition was calculated to ensure complete coordination of the metal ions with both the M and G residues of the alginic acid solution. Then mixture was then transferred to a glass beaker with water (7gm of powder mixture in 20gm of water) and agitated for 4 hours at 80°C, to obtain NaAlg solution in water. This solution was subsequently oven-dried and pulverized to obtain NaAlg powder. Similarly, for the preparation of LiAlg, NaOH was replaced with $LiOH \cdot H_2O$ and the rest of the method was followed, to obtain LiAlg powder.

3.1.2. Physical Characterization

Visual observations and characteristics

Fig. 3.1 shows the visual differences between the synthesized and commercial NaAlg powders. The synthesized NaAlg powder also produce a slight odour of caramel - indicting minor physio-chemical changes in the polysaccaride structure caused due to the drying process.

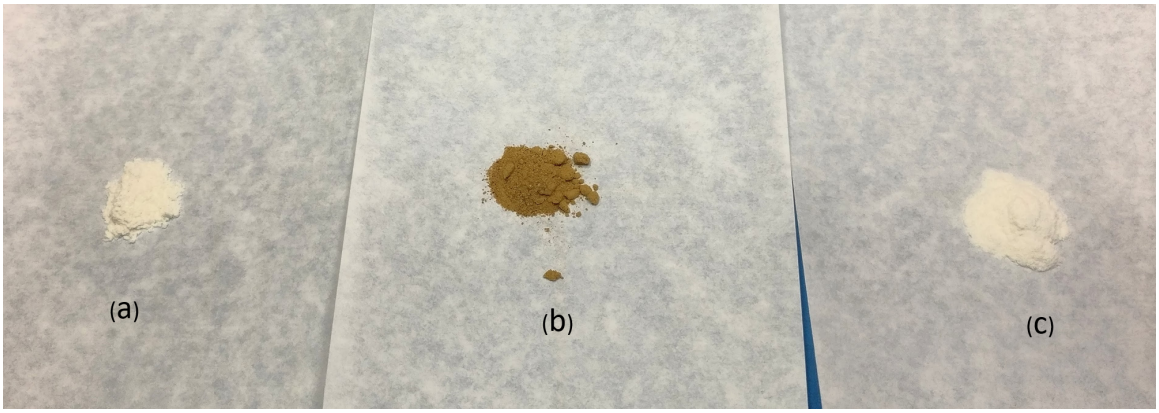

Figure 3.1: Visual comparision of the NaAlg salts.
(a) Base Alginic Acid
(b) Synthesized NaAlg salt
(c) Commercial NaAlg salt

In a comparative visual study, it was observed that the the aqueous solutions prepared from the commercial NaAlg powder yielded a higher viscosity solution at the same salt concentration as the synthesized powder. The observed difference in viscosity is theorized to be the result of the difference in polymer chain length of the AlgA (used as the base in synthesis method) and the AlgA used in the commercial production of NaAlg. According to Fertah et al. [33], the M/G ratios of alginates and the block structure are crucial in determining the physico-chemical properties of alginates. Donati et al. [34] reported that the monomer sequence (M and G) can differ among algal species and also in different tissues of the same species, which is possible the reason for the evident viscosity differences. For the commercial NaAlg, it was observed that the could also processed into free-standing films and also gel polymer electrolytes (GPEs) (refer appendix, Fig. A.1) with high salt concentrations. The synthesized NaAlg powder, on the other hand, formed brittle films. Penman et al. [35] reported that brittle gels are obtained from alginates with a low M/G ratio, while elastic gels are formed from alginates with a high M/G ratio. Thus, the commercial NaAlg would serve as more suitable candidate for preparing electrolytes, and was decided to be used in the scope of Na systems. However, the flexibility of the preparation method needs to be studied. Therefore, both the synthesized and commercial NaAlg powders were subjected to further characterization using FTIR.

In the case of LiAlg, the synthesized powder is obtained (Fig. 3.2) similar in colour to the synthesized NaAlg powder. In further similarity, the LiAlg had poor gelation properties, but could be processed into highly concentrated aqueous solutions. It was also observed that the gels and coatings made using these alginates were brittle (refer appendix, Fig. A.2). These observations are similar to those by Santhosh Shetty in his work on the feasibility of Alginate Polymer Electrolytes through Molecular Dynamics Simulations.

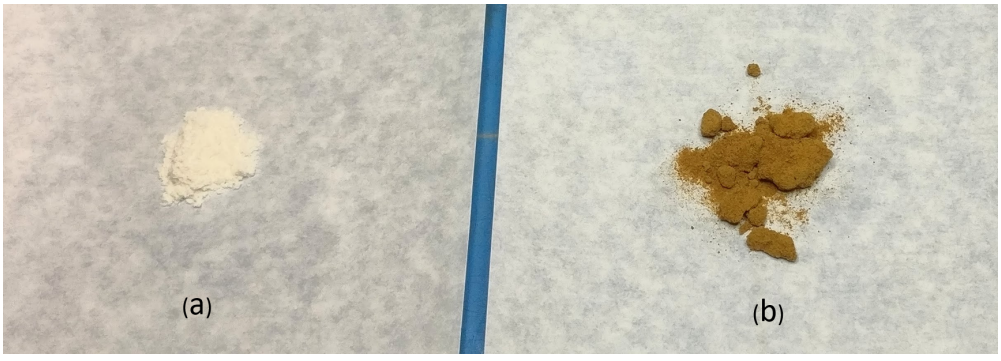

Figure 3.2: Visual comparison of the LiAlg salt.
(a) Base Alginic Acid
(b) Synthesized LiAlg salt

Fourier-Transform Infrared Spectroscopy (FTIR) analysis

Further characterization of the synthesized powders was done through Fourier-transform infrared spectroscopy (FTIR). FTIR is a technique used to obtain an infrared spectrum of absorption or emission of a solid, liquid or gas. An FTIR spectrometer emits IR light through a sample to a detector. The detector measures the light to determine which wavelengths were absorbed. This data is then turned into an absorbance (or transmittance) spectrum using a Fourier transform.

Device: Thermo Scientific Nicolet iS50 FT-IR

The FTIR characterization, in this study, was performed for four samples - the commercial AlgA as a baseline, the commercial NaAlg, the synthesized NaAlg and the synthesized LiAlg. To perform the FTIR measurements, a mixture of the powder under analysis and potassium bromide (1:10 proportion by volume) is thoroughly dispersed using a pestle and mortar. This powder is placed in a pellet-die set and then subjected to compression at 7.5 tons for three minutes using a hydraulic press. This turns the powder into a transparent pellet that can then be used to measure an FTIR spectrum.

As mentioned earlier, to investigate the flexibility of the alginate salt synthesis method, FTIR was first performed between the baseline AlgA, the synthesized and the commercial NaAlg. From Fig. 3.3, it can be seen that the IR spectra for the commercial and synthesized NaAlg are very similar to each other with minor variation caused due to moisture and CO_2 in the test chamber. The highlighted regions of the plots show the characteristic peaks of NaAlg and their variation from the base AlgA. In accordance to the study by Huang et al.[36], the most significant difference between NaAlg and AlgA is observed at around 1400cm^{-1} (in the gray region of the plot), which signifies the symmetric stretching vibration of the (COO^-) caused due to Na coordination. Another distinction between AlgA and NaAlg is observed in the 1550 to 1750cm^{-1} range. In the NaAlg, the existence of the carbonyl group in the carboxylate anion form causes an inverse peak at 1600cm^{-1} while in case of the AlgA, the carbonyl group exists as a carboxylic acid (in ester form) responsible for the inverse peak at 1730cm^{-1} (in the blue region of the plot).

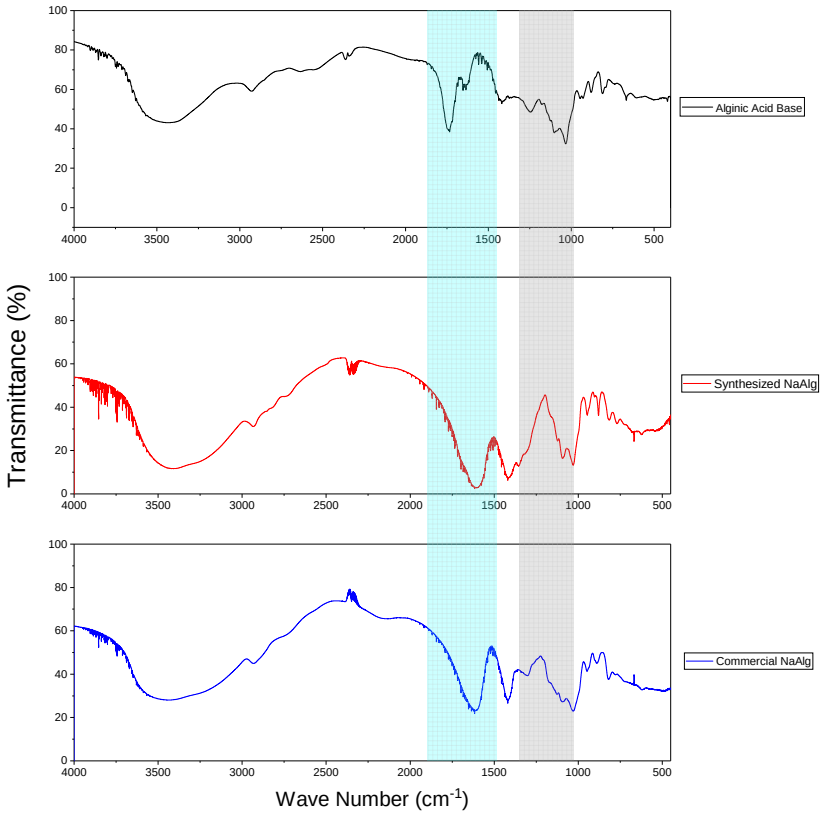

Figure 3.3: FTIR spectra for
(a) base alginic acid
(b) synthesized NaAlg
(c) commercial NaAlg

The IR spectra for both the NaAlg samples are collinear, which ascertains the flexibility of the synthesis method. The matching spectra also removes concern about the difference in colour of the two samples. The physio-chemical reaction caused on drying appears to have insignificant effect on the spectra, adding further merit to the synthesis.

Subsequently, FTIR was conducted between the baseline AlgA, the synthesized LiAlg and the commercial NaAlg. From Fig. 3.4, it is immediately evident that the spectra for LiAlg and the commercial NaAlg are extremely similar, with characteristic peak at 1400cm^{-1} (in the gray region of the plot) caused due to Li^+ coordination as well as the shifting of the carboxyl group inverse peak to 1600cm^{-1} (in the blue region of the plot). This is expected as both the alginate salts have a similar structure since both Li^+ and Na^+ ions coordinate in identical manner with AlgA. It can also be observed that the 1400cm^{-1} peak is less pronounced in the case of LiAlg as compared to the NaAlg, although this is possibly due to experimental error.

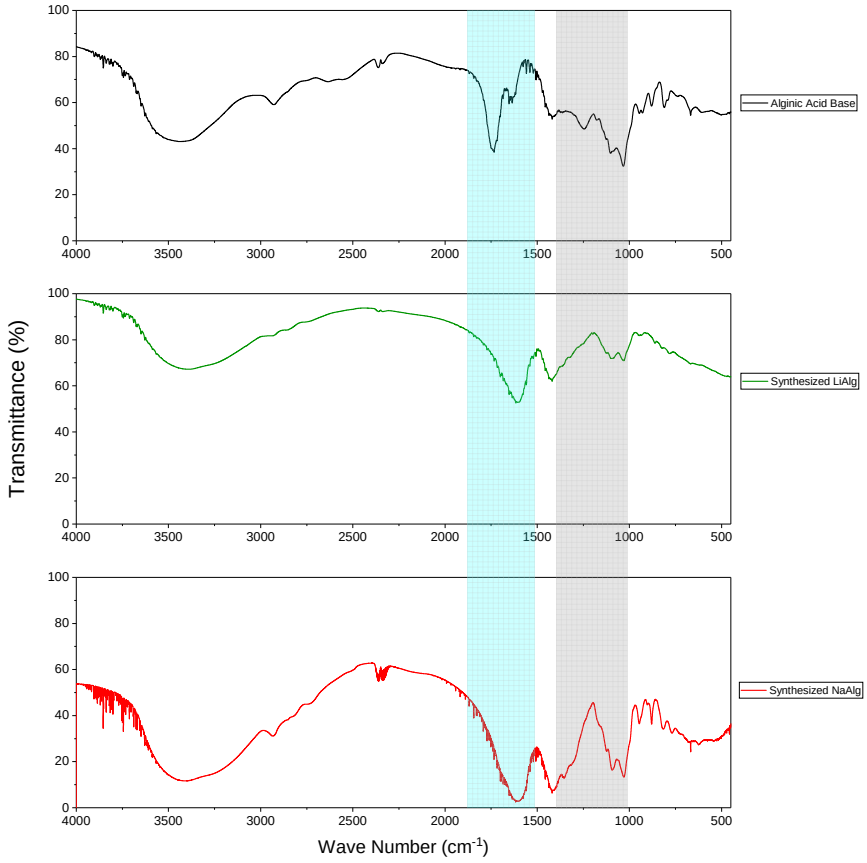

Figure 3.4: FTIR spectra for
(a) base alginic acid
(b) synthesized LiAlg
(c) synthesized NaAlg

3.2. Lithium Aluminium Germanium Phosphate (LAGP)

For the scope of LiAlg, the Li-SSE chosen was LAGP. Traditionally, solid-state synthesis is used to prepare inorganic solid electrolytes. In these methods, the precursors chemicals are initially mixed and ball milled for better dispersion. Subsequently, the mixed powder is subjected to a solid-state reaction and densification through sintering heat treatments, which usually require high temperatures (700–1200°C) and long dwell times [6]. The high temperature also assists in reducing grain induced resistances. In this work, a similar synthesis method is employed for the preparation of LAGP powder.

3.2.1. Powder and pellet synthesis

Required Chemicals:

The precursors materials required for the preparation of LAGP powder are mentioned below:

Chemical	Supplier	CAS
Lithium Carbonate (Li_2CO_3) [37]	Sigma Aldrich	554-13-2
Germanium Oxide (Ge_2) [38]	Sigma Aldrich	1310-53-8
Aluminium Oxide (Al_2O_3) [39]	Sigma Aldrich	1344-28-1
Ammonium di-Hydrogen Phosphate ($(NH_4)H_2PO4_3$) [40]	Sigma Aldrich	7722-76-1

Method: Fig. 3.5 shows a schematic description of the preparation method used for the LAGP powder and pellet.

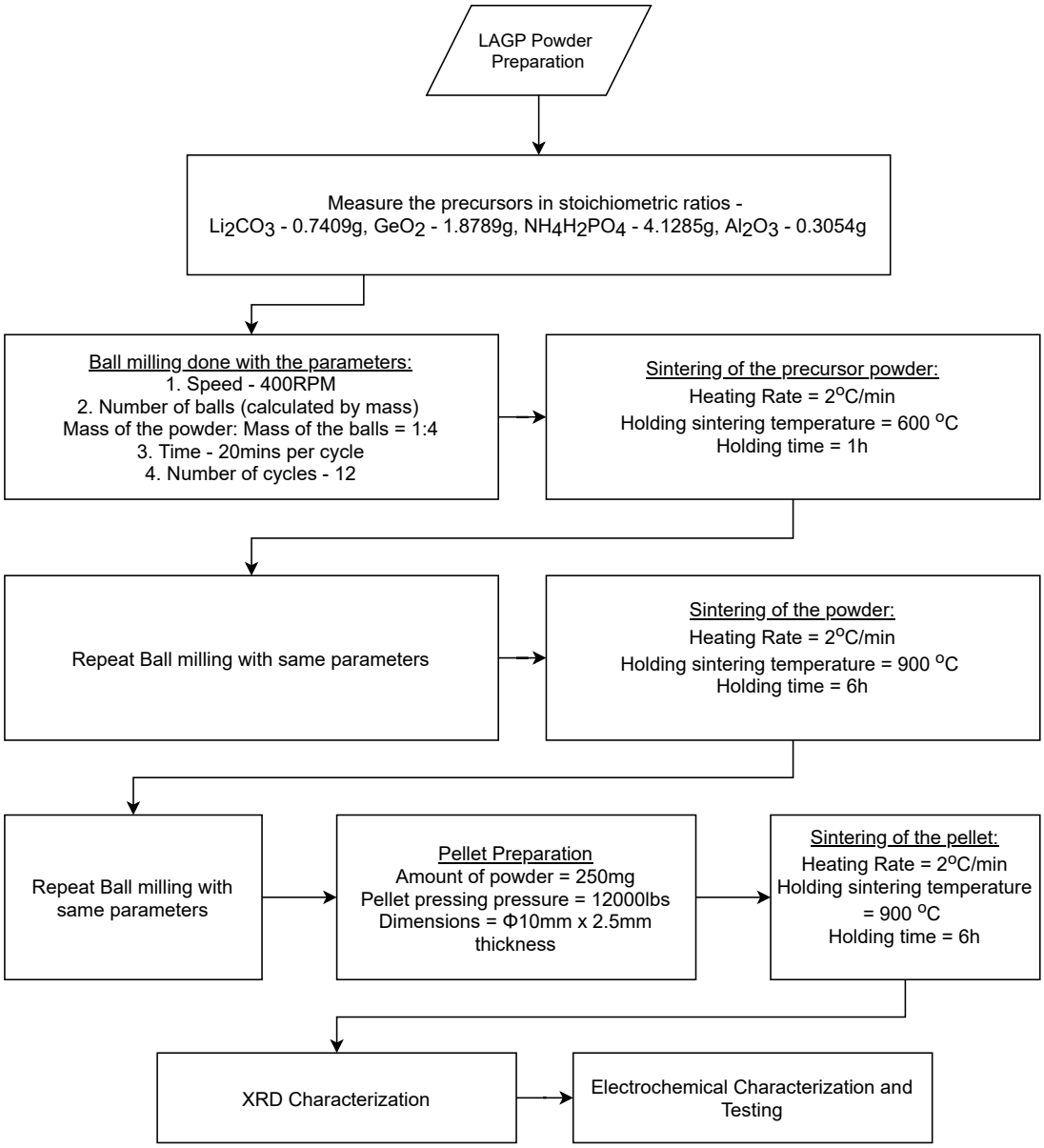

Figure 3.5: Schematic representation of solid-state synthesis of LAGP powder

3.2.2. Physical Characterization

Visual observations and characteristics

The synthesized powder and pellets were (Fig. 3.6) were subjected to physical characterization before electrochemical experiments were carried out.

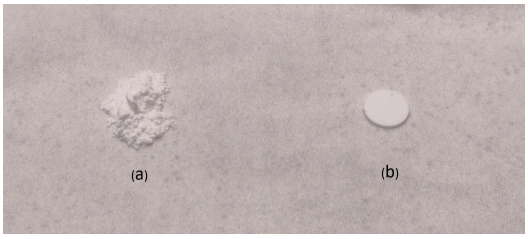

Figure 3.6: Visual observations of (a) LAGP powder after final ball milling
(b) LAGP pellet after sintering

The physical characterization of the prepared LAGP powder was done by using X-Ray Powder Diffraction (XRD) and Scanning Electron Microscopic (SEM) techniques.

X-Ray Powder Diffraction

XRD is a characterization technique based on optical scattering, used for the investigation of crystalline materials. X-rays are generated in a cathode ray tube by heating a filament to produce electrons. The electrons are then accelerated towards a target by applying a voltage. When the electrons have sufficient energy to dislodge the inner shell electrons of the target material, a characteristic X-ray spectrum is produced. This spectral data is then compared to standard reference spectra to identify the materials [41].

Device: X'Pert Pro PANalytical

LAGP consists of $LiGe_2(PO_4)_3$ (LGP) as the main phase, with partial replacement of the Ge^{4+} ions by Al^{3+} ions. $AlPO_4$ is the most common secondary phase obtained after the synthesis process. It is amorphous and forms a barrier layer at the grain boundaries of LAGP. Other minor impurities include $Li_4P_2O_7$ and GeO_2 mainly owing to the evaporation of Li^+ [6, 11]. Fig. 3.7 shows the XRD spectra for three different samples - the LAGP powder after the synthesis (in red), the LAGP pellet after the sintering (in green) and a commercially available LAGP powder(in blue, Supplier: MSE Supplies[42]). It can be observed that all the three spectra match up with each other with the synthesized powder and pellet showing a dominant LAGP phase with minor quantities of the $AlPO_4$ and GeO_2 impurities.

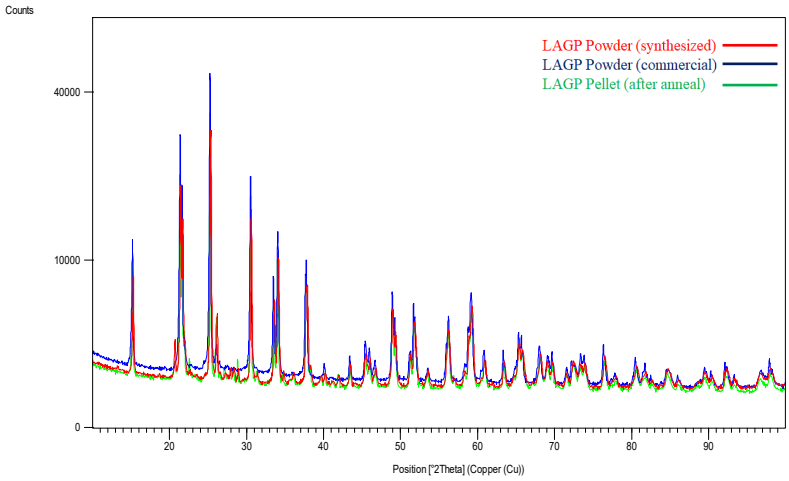

Figure 3.7: Comparative plot of XRD spectra from the three different LAGP samples

Scanning Electron Microscopy

A scanning electron microscope (SEM) is a type of electron microscope that produces images of a sample by scanning the surface with a focused beam of electrons. The electrons interact with atoms in the sample, producing various signals that contain information about the surface topography and composition of the sample.

Device: JEOL JSMIT100 with EDXS

Fig. 3.8 presents the surface SEM imaging for an LAGP pellet which depicts the microstructure and surface morphology of a sintered LAGP pellet. These images are in accordance with existing literature, with a dense packing of a large number of cube-shaped crystals with evidence of porosity in the microstructure [43, 44].

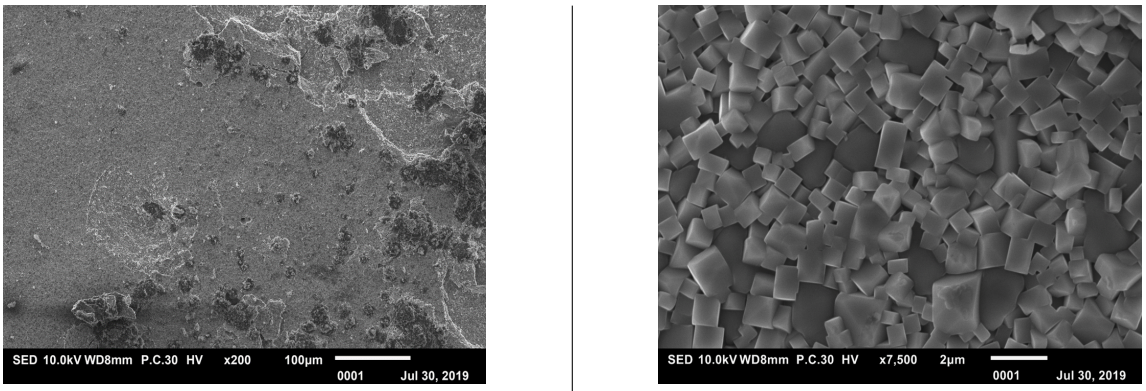

SEM at low magnification

SEM at higher magnification

Figure 3.8: SEM image of the surface of a LAGP pellet at different magnifications

3.3. Testing configurations

In the duration of this study, the different material were required to be processed into different test configurations. This section aims to discuss the preparation of these various test configurations.

3.3.1. Electrode slurry and cell preparation

The conventional procedure for the preparation of Li-ion battery electrodes includes mixing the active material with conductive carbon additives and a polymeric binder dissolved in a solvent to form a slurry of the electrode mixture. The mixing is done for about 4hrs after which the produced slurry is cast on metal foil current collectors using the doctor blade method and dried. After the drying, the coatings are cut into square samples, which are then pressed at a certain pressure using a hydraulic press - to control the electrode porosity and to improve the adhesion of the coating to the substrate.The pressed electrode sheets are then cut into circular electrodes (usually ϕ12.7mm) after which the electrode thickness and weight are measured. The prepared electrodes are then subjected to a final drying overnight, this time in a vacuum to remove traces of solvent and moisture. The dried electrodes are then transferred into an argon glove-box, for cell preparation. The measurements taken earlier are used for calculating properties of each electrode such as active material mass, specific capacity, areal capacity, active mass density and porosity of the electrode.

Depending on the testing configuration, coin cell and solid state cells were prepared for the electrochemical testing. For coin cells (Fig. 3.9), half cells were assembled against Li^+ or Na^+. For the experimental work done in Section 4.5 and Section 5.2, most electrodes (LFP, NMC, LNMO, LTO (Lithium titanium oxide, $Li_4Ti_5O_{12}$), Si, NMO, NaTP) have been prepared with an 80/10/10 proportion (active material/carbon black/PVdF binder in NMP solvent). The Si/graphite composite electrodes were prepared with 85% graphite/5% Si/2% CB/3% CF/5% PVdF. Copper, Aluminium and Stainless steel mesh (SS) were used as the substrate for the anode, cathode and aqueous electrodes respectively.

Some testing has been done in organic liquid electrolyte, in which case 1M $LiPF_6$ in EC:DEC 1:1 + 2% VC has been used in Li^+ systems while 1M $NaClO_4$ in EC:PC 1:1 has been chosen in Na^+ systems. Additionally

in the Na^+ system, a common aqueous electrolyte - 1M Na_2SO_4 in water is used for aqueous electrodes. For testing solid-state pellets and gel-polymer electrolytes, the testing components were assembled in solid state cells (Fig. 3.10). Additionally, NaAlg and LiAlg were tested as binders in a Si/graphite composite system and compared against some conventional anode binders (PVdf, CMC/SBR, PAA and Li.PAA).

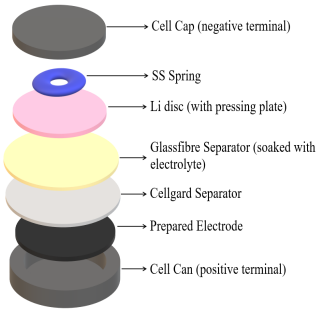

Figure 3.9: Exploded view of a coin cell

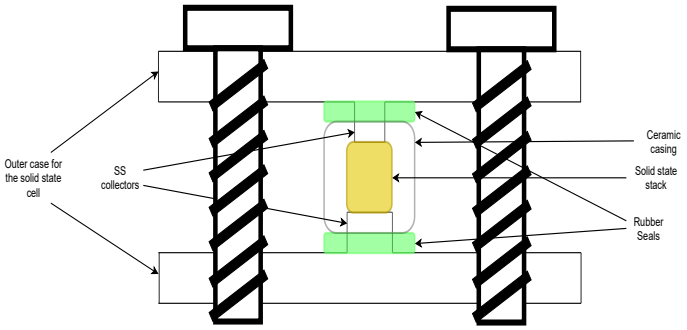

Figure 3.10: Cross sectional view of a solid state cell

3.3.2. Electochemical Impedence Spectroscopy

Device: Metrohm Autolab PGSTAT12

Electochemical Impedence Spectroscopy (EIS) is a characterization method used to measure the impedance of an electrochemical system by recording the current response to an applied potential at varying frequencies. The impedance of an electrode/electrolyte/electrode system is investigated by subjecting the system to an AC voltage of 1-10 mV (with frequencies between 1 mHz and 1 MHz) on top of the controlled DC voltage (usually at open circuit potential). The nyquist plot is then obtained by plotting the negative of the imaginary part of impedance versus the real part for the different frequencies. These plots usually consists of one or more semicircles at high frequencies (where the ionic transport is kinetic controlled) followed by a spike at low frequencies (where the ionic transport becomes mass transfer controlled, giving rise to diffusion from the surface known as the "Warburg" impedance). EIS data are commonly analyzed by fitting the curve with an equivalent electrical circuit model to understand the contribution from each interface or bulk process [45].

A general nyquist plot for a electrochemical system is shown in Fig. 3.11, which can be fitted as shown in Fig. 3.12. In this equivalent circuit, R_{el} represents the electrolyte resistance, C_{dl} represents the double-layer capacitance, R_{ct} represents the charge transfer resistance and W represents the Warburg element which describes the mass transport of the electroactive species (diffusion in the electrode-electrolyte interface).

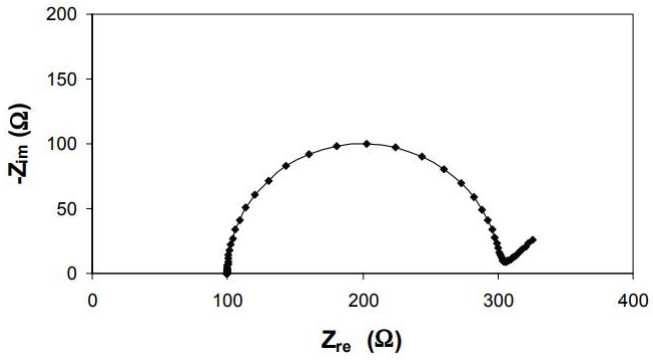

Figure 3.11: Conventional nyquist plot for mixed-control systems

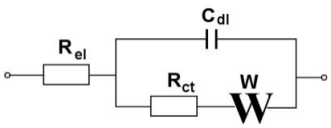

Figure 3.12: The equivalent electrical circuit

The electrolyte resistance R_{el} obtained from the EIS nyquist plot can then be used to calculate the conductivity of

the electrolyte using the equation:

$$\sigma = \frac{L}{A} \times \frac{1}{R_{el}}$$

where σ is the electrolyte conductivity (in S/cm), L is the distance between the electrodes where the electrolyte is present (in cm) and A is the contact area between the electrodes and electrolyte (in cm^2). In this study, EIS measurements have been utilized to determine the electrolyte conductivity and interfacial resistance in different configurations. Symmetrical cells with blocking Stainless Steel (SS) electrodes, conductive electrodes (Li or Na) and for full cell configurations (Section 5.2).

3.3.3. Cycling and Rate Capability Testing

Device: Maccor Series 4000 Automated Test System

For the rate capability experiments (in Section 4.5), half cells (coin cells) were prepared from various electrodes and were subjected to various rate capability test in the Maccor system. These rate capability tests were generally performed for various C rates, increasing from C/20 to 10C before decreasing to C/20 - such testing would shed light into the ability of the electrodes to resist the stresses caused due to the different C rates as well as determine the irreversibility of capacity losses. The baseline cycling tests done for NaAlg aq. electrolytes (including the Na_2SO_4 and the GPE, in Section 5.3) were assembled in swaglok-type cell (known as lab cells) and the solid state cells respectively (refer appendix for a schematic view of assembly of the GPE system, Fig. A.3). The electrolytes were pressed inside the testing cells with NMO cathode and NaTP anode and cycled between 0.1 and 1.2V.

3.3.4. Testing configurations for LiAlg and LAGP

As discussed earlier, after the preparation of the LiAlg powder, attempts to make films and pellets proved unsuccessful. Therefore to perform conductivity measurements, a 20w% LiAlg aq. solution was prepared by mixing the respective amounts of LiAlg and water in a beaker with mechanical agitation for 4hrs. This solution was then cast onto a highly absorbant glass fibre separator till soaked and oven-dried. This dried separator was then utilized for the baseline EIS measurements.

For evaluating the performance of LiAlg on LAGP, the same solution was used to cast a thin layer of LiAlg on the surface of the LAGP, oven-drying and repeating on the other side. The final dried pellet (Fig. 3.13) was then subjected to EIS measurements.

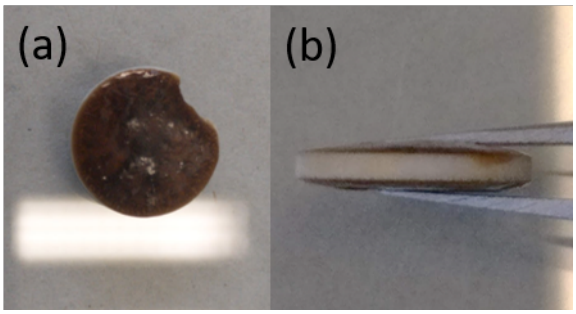

Figure 3.13: LiAlg coated LAGP
(a) top view
(b) side view

For further understanding the performance of the LiAlg coating, the various electrodes were prepared as discussed earlier and the LiAlg solution was drop-casted on the electrode to prepare a secondary electrolyte layer. These electrodes were assembled into coin cells with the Li liquid electrolyte and the performance of the coating was evaluated.

3.3.5. Testing configurations for NaAlg

Due to the better physical characteristics of the commercial NaAlg, the same had been used from the Na-ion scope of this study. For conductivity measurements discussed in Section 5.1, NaAlg pellets were prepared with different water concentrations. The 2w% aqueous solution (and the 5w%) solutions were prepared by dissolving 0.2g (and 0.5g resp.) in 9.8g (and 9.5g) of water. The solution was agitated for 4H using a stirrer for uniform concentrations. For the gel polymer concentrations (10w% and 20w%), 1gm batches of the electrolyte were prepared by mixing the relative amount of NaAlg and water (0.1-0.2gm of NaAlg with 0.9-0.8gm of water resp.) in a pestle and mortar to fully incorporate the water into the powder (similar to bread dough preparation). For the solid state concentrations (50w%, 75% and 100w%), 100mg batches of the electrolyte were prepared by mixing the relative amount of NaAlg and water (50, 75 and 100mg of NaAlg with 50, 25 and 0mg of water resp.) in pestle and mortar. The powders were then placed in a ϕ6mm die-pellet set and pressed to 5 tons in a hydraulic press (with a hold time of 2 min). This yielded pellets of about 2mm thickness (Refer appendix, Fig. A.1). For the thickness-dependent conductivity measurements, 100w% NaAlg pellets were utilized with a constant ϕ6mm. The 0.1mm thick film was prepared by casting 50mg of the 2w% NaAlg aq. electrolyte onto a glass substrate and oven-drying the cast (for 2hrs) till a peel-able film is obtained. The other pellets (0.53, 1.82 and 2.5mm thick) were prepared by using 50mg, 100mg and 150mg of dry NaAlg powder pressed in the ϕ6mm die-pellet set to 5 tons.

4

Experimental work with Lithium Alginate and LAGP

This chapter mainly discusses the results of the experiments carried out with LiAlg and LAGP. But firstly, the scope of alginate salts as binders has been investigated and compared with conventional ones in anode systems. Then, proceeding onto the LiAlg scope, the ionic conductivity of LiAlg is estimated including the effect of prolonged Li contact, proceeded by similar trials for LAGP. Then, the effect of the LiAlg coating on LAGP is discussed. Further, to simplify the system, the LiAlg coating is isolated from the LAGP, by applying it onto conventional electrodes and a liquid electrolyte to study the rate capability and performance of such a coating. A proof of concept is hence established for the LiAlg coating as a secondary electrolyte.

4.1. Alginates as binders

As most of the research into alginates has occurred in the form of polymer binders in anode system, it was decided to first use the synthesized LiAlg and the commercial NaAlg powders for a comparative study with other binder systems. The testing environment used was silicon/graphite composite anode and the comparison was done against CMC/SBR, PVdF, PAA and Li.PAA (Lithium salt of polyacrylic acid). PVdF was included as the conventional binder for anode systems (with a majority of graphite concentration. CMC/SBR, PAA and Li.PAA are aqueous binders and have been observed to provide better binding and improved capacity upon cycling by limiting the cumulative irreversible losses induced in Si anodes. The comparison of NaAlg and LiAlg with CMC/SBR, PAA and Li.PAA would be of great interest due to the similarities in improved properties caused by functionalized polymers.

Half cells were prepared (as explained in Section 3.3) and cycling tests were carried out for the different binder systems. Fig. 4.1 shows the capacity fade in the electrodes. It can be observed that the aqueous binders perform better than the PVdf binder system, reaffirming the benefits of functionalized polymers. The performance characteristics for the tested electrodes follow the trend: NaAlg > Li.PAA > PAA > LiAlg ≈ CMC/SBR > PVdF. The NaAlg binder system experienced least capacity fade and has a final stable capacity higher than the theoretical graphite capacity. The LiAlg on the other hand experienced higher capacity fade and a slightly lower stable capacity. Nevertheless, the improvement over PVdF is clear and establishes the merit of alginate salts as viable alternative binders.

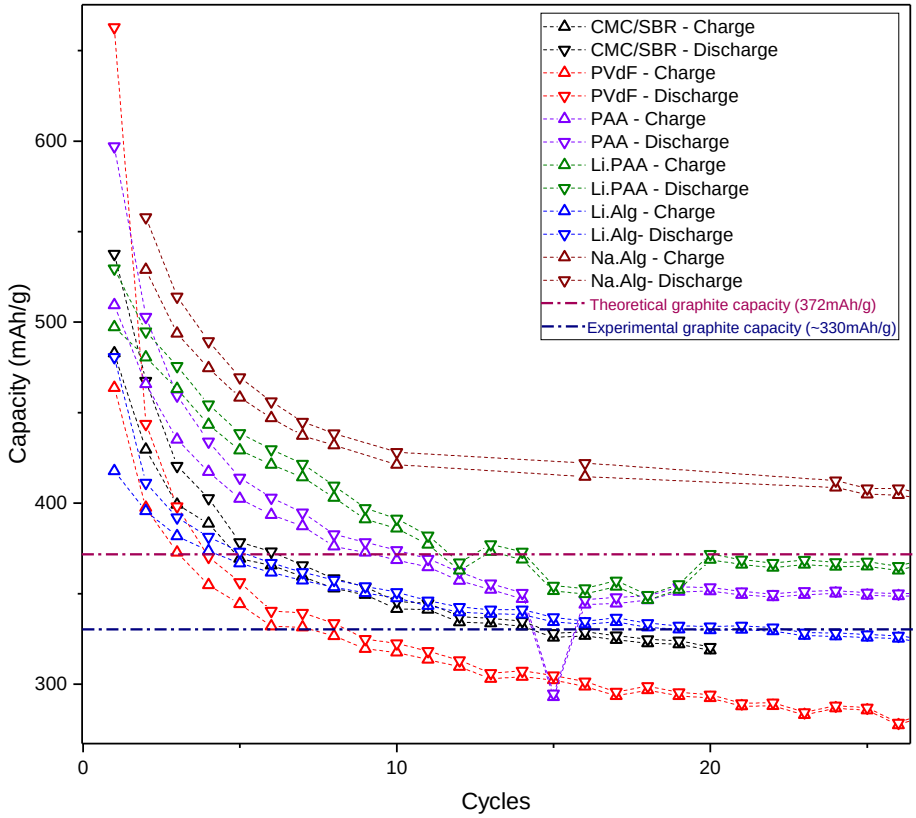

Figure 4.1: Comparison of the rate capability performance of Si/C anodes in different binder systems

4.2. Electrochemical performance of LiAlg

For calculating the conductivity of the LiAlg soaked separator, it was subjected to EIS measurements in symmetrical SS systems (refer appendix, Fig. A.4) and with Li systems. In both the systems, the conductivity was measured at 0.2 mS/cm, which is in the same margin as conventional SSEs. Additionally, the LiAlg separator was left in contact with Li over 48hrs to observe the effect of prolonged Li metal contact. The EIS measurement taken after 48H exhibited a minor decrease in conductivity to ≈ 0.1 mS/cm.

On the disassembly of this cell, it was observed that the Li foil has oxidized to form white LiOH (Fig. 4.2) on the side which was in contact with the LiAlg separator. This is possibly due to the reaction of the Li metal with the inherent polar bonded water molecules on the surface of the LiAlg pellet. This reaction is accelerated by the concentration gradient of water in the LiAlg bulk and the ability of LiOH to conduct Li ions causing fresh Li continuously being exposed to the water at the LiAlg surface. The conclusion from the measurements is that the continued formation of the LiOH layer is detrimental to the interfacial performance (refer appendix, Fig. A.5).

Figure 4.2: Formation of white LiOH on Li foil on prolonged contact with LiAlg

4.3. Electrochemical performance of LAGP

Subsequently, after the electrochemical trials with LiAlg and the physical characterization of LAGP, the focus was shifted to establish similar baseline electrochemical characteristics for LAGP including the impact of prolonged Li contact on the pellet surface.

4.3.1. Conductivity measurements for LAGP

For the baseline conductivity measurements for LAGP, EIS measurements were carried out with the pellets in the SS and Li systems (refer appendix, Fig. A.6). In this case, the conductivity was calculated at 0.5mS/cm in both the systems, these calculations are in line with those observed in literature [6].

4.3.2. Li-induced decomposition of LAGP

As mentioned in earlier sections, it has already been established in literature that LAGP electrolyte undergoes decomposition reactions on contact with Li metal. To study this behaviour, the Li/LAGP/Li system was kept for 48hrs and EIS measurements were carried out as can be observed from Fig. 4.3. The bulk electrolyte resistance and thus conductivity of LAGP remains the same, meaning that the decomposition layer has limited adverse effect on the bulk ionic conductivity. However, at the low frequency part of the EIS data corresponding to interfacial resistance, there is evidence of decreasing conductivity over the interface.

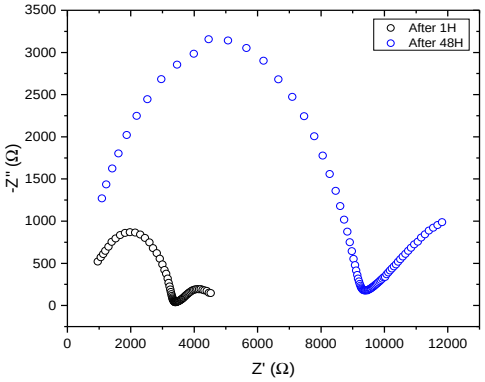

Figure 4.3: EIS comparison for a Li/LAGP/Li system
O - 1hr after assembly
O - 48hrs after assembly

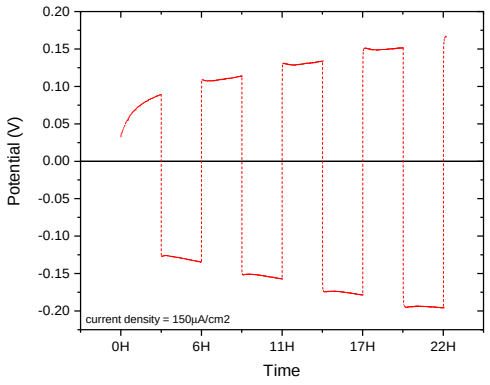

Figure 4.4: Galvanostatic cycling of the system at increasing current densities

Disassembling the cell, it was also observed that the LAGP pellet had developed deep cracks and lost its mechanical integrity. For further studying the degradation, a new Li/LAGP/Li cell was prepared and subjected to galvanostatic cycling at a constant current density. From Fig. 4.4, it was observed that the over-potential increases with increasing cycles. This establishes that the degradation mechanism of LAGP with Li is both chemical and electrochemical in nature. Further, these observations are accordance to the study conducted by Tippens et. al[46], where the analysed the chemo-mechanical degradation caused on LAGP electrolytes on Li metal contact. They reported that the formation of the decomposition layer does not harm ionic or electronic transport, but it is the cracks that result from the growth of the interfacial layer that accelerate the degradation of the electrolyte.

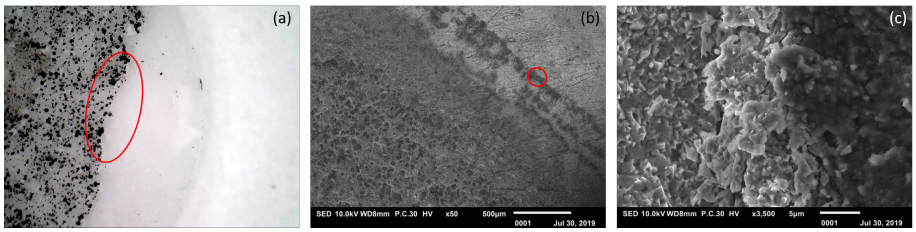

Figure 4.5: Surface SEM of the LAGP pellet
(a) The white region is the bare pellet and the black region is the area of the pellet that was in contact with the Li. [highlighted region focused in (b)]
(b) Contrast in the region in contact with the Li (darker) and the bare pellet. [highlighted region focused in (c)]
(c) Bare pellet (on the left) retains the usual cubic particle structure while the Li contact causes the chemical degradation evident (on the right)

.

Observing the same pellet using SEM provides some visual information on the decomposition. Fig. 4.5(c) shows the contrast in surface morphology in the reacted and pristine regions of the LAGP pellet. To maintain the mechanical integrity of the LAGP pellet, it is essential to avoid direct contact with Li. To achieve this, trials were conducted by coating LiAlg on the pellet's surface and similar experiments were carried out.

4.4. LiAlg coated LAGP - Effect of Li contact

After the performance studies on LiAlg and LAGP, the LiAlg coated LAGP pellet was prepared as mentioned earlier (Fig. 3.13). As done for the bare LAGP pellet, EIS measurements were performed with SS blocking electrodes and Li electrodes. The EIS nyquist plots show erratic impedance curves which is possibly due to contact issues cause by the brittle LiAlg coating. Nevertheless, conductivity measurement of the pellet in both electrode systems was calculated as 0.4mS/cm, indicating that the presence of the coating does not hamper the conductivity of the LAGP electrolyte. Subsequently, the Li system was left undisturbed for 48hrs to observe the effect of prolonged Li contact. EIS measurement conducted for the system after 48hrs showed similar conductivity values. However, in contrast to the bare LAGP pellet (Fig. 4.3), the LiAlg coated LAGP pellet displayed significantly better interfacial resistance after prolonged contact as can be observed from Fig. 4.6. The pellet was disassembled to observe the condition of the pellet. It was observed that there were only minor traces of reaction on the surface of the Li foil and on the LiAlg layer. This is in contrast to the LiAlg soaked separator where LiOH formation was observed.

A possible reason for this observation could be that the combination of the LiAlg and LAGP causes kinetic hindrance to the continual diffusion of water through the LiAlg bulk into the Li. The hygroscopic nature of the LAGP could be playing a role in countering the water diffusion away from the LiAlg restricting the formation of LiOH only at the surface. Additionally, the LAGP pellet remained mechanically stable, even though there was minor mechanical damage to the LiAlg coating (possibly caused due to the clamping pressure coupled with the brittleness of the LiAlg layer). The LiAlg and LAGP thus performed as protective elements to each other's degradation mechanism with Li.

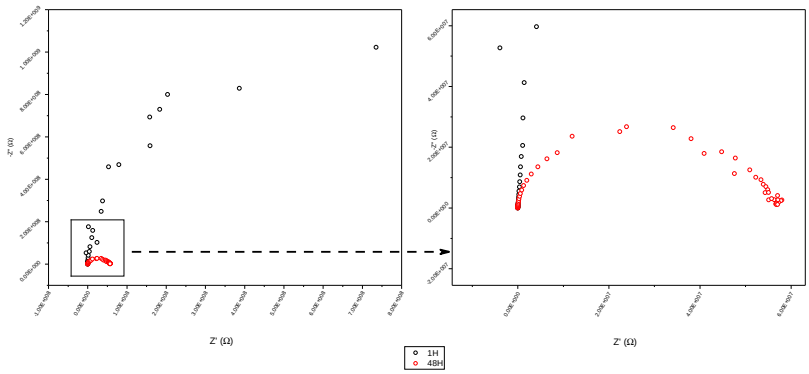

Figure 4.6: EIS Comparison for the LiAlg coated LAGP in Li systems
O - 1hr after assembly
O - 48hrs after assembly

4.5. LiAlg as a coatings on electrodes

The experiments with the LiAlg coated LAGP look promising, however due to the presence of multiple electrolytes and interfaces, it is required to simplify the system to fully understand the scope of the LiAlg coating. For this purpose, it was decided to cast the LiAlg as coatings on various electrodes to be tested with liquid electrolyte against Li. The reasoning behind these experiments were:

- Isolating the LiAlg from the LAGP would help in obtaining a better understanding of its Li-ion conduction and its performance as a secondary polymer electrolyte.
- A high interfacial resistance is observed in the LiAlg coated LAGP system, but the reason is unclear. By testing the interfacial performance of LiAlg coated electrodes against LE, it would be easier to pin-point the cause of the high interfacial resistance.
- By performing the rate capability testing of these electrodes, it would also be possible to observe the capacity performance and thus the protective nature of these coatings. High rate testing would also subject the LiAlg coating to high cycling-induced stresses and the performace would give more information on the electrochemical stability of the coatings.

The coatings were prepared as mentioned earlier and Fig. 4.7 shows a surface SEM of two NMC cathodes, with and without the LiAlg casting.

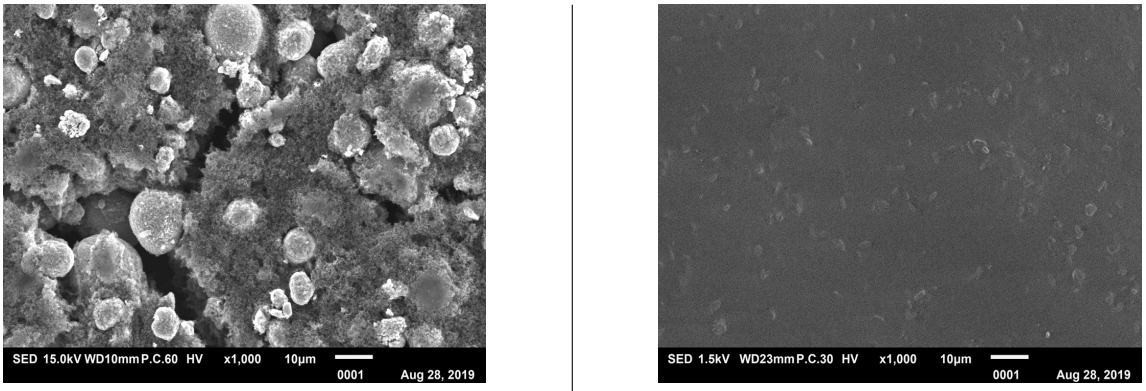

Bare NMC cathode | Coated NMC cathode

Figure 4.7: SEM image of the surface of a coated and a bare NMC cathode

It is evident from these images that the LiAlg casting has occupied a majority of the electrode porosity as well as uniform coverage on the surface. Thus, in essence, the LiAlg will serve as a second electrolyte and provide a conductive matrix within the bulk of the electrode (refer Fig. A.7 for a schematic representation). Subsequently, half cells were prepared for these coated electrodes to compare their performance against similar electrodes without the coating. Various electrodes (NMC, LFP, LMNO, Si/C composite, Si and LTO) were chosen for studying the LiAlg performance in different cycling windows. The results of these experiments for all the different systems are similar (refer appendix, Fig. A.8 to Fig. A.17) and can be be understood by observing the performance of any one system. The observations for the NMC system are discussed subsequently.

LiAlg coated on NMC electrodes

As discussed in Section 3.3, NMC electrodes were prepared and characterization, with few electrodes casted with LiAlg on the surface of the electrode. The LiAlg layer extended upto $\approx 10\mu$m above the electrode surface. These electrode were also dried and assembled into coin cells. The cells were the subjected to the rate capability tests to observe the impact of different current densities on the performance of the cell.

Fig. 4.8 shows the cycling curves for both the electrodes at C/20 rate. It can be observed that the coated electrode observes slightly longer charging/discharging times - which might be due to delayed ion conduction through the LiAlg layer. Fig. 4.9 shows the average capacity (charge and discharge) at different C rates. The average

capacities are compared due to high coulombic efficiencies (≈97%) at the different C rates. From Fig. 4.9, it is clear that the coated electrode displays slightly higher capacities as compared to the bare ones. It is also evident that there is capacity loss at higher C rates, the decrease in capacity appears to be more drastic in case of the coated electrode. On returning to lower C rates, it is promising to note that the electrodes regain most of their lost capacity. It can be concluded from these graphs that the LiAlg coating provides good Li^+ ion conducting performance at the electrode surface as well as through the electrode bulk.

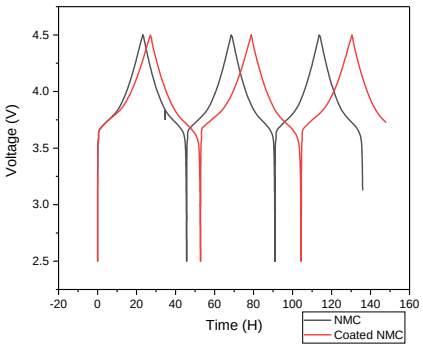

Figure 4.8: Comparison of cycling curves for the coated and bare NMC electrodes at C/20 rate

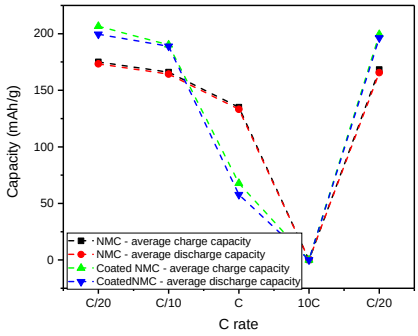

Figure 4.9: Capacity variation with C rate for the coated and bare NMC electrodes

EIS measurements (refer appendix, Fig. A.18) were carried out for the two cells for impedance characterization and the electrolyte conductivity was calculated. The conductivity was observed to decrease from 4 mS/cm to 2 mS/cm in presence of the LiAlg coating. This further consolidates the hypothesis that Li conduction is slower in the presence of the LiAlg coated. Another interesting observation from the EIS plots are the interfacial resistances. The interfacial resistance observed in the case of the LiAlg coated electrode is slightly higher than that of the bare electrode, which is expected. However, the values are within the same margin for those between electrodes and liquid electrolytes. These results are observed for the Si/C composite anode as well Fig. A.19). Thus, as a proof of concept, these observations support the excellent scope of LiAlg as electrolytes.

Similar characteristics have also been observed for the cycling trials conducted with the other electrodes. Therefore, it can be concluded that the LiAlg coating shows excellent performance as a secondary polymer electrolyte and is a viable pathway into successful solid-state batteries.

4.6. Inferences from experimental trials with LiAlg

- LiAlg and NaAlg show excellent performance in capacity retention as binders in Si/C composite anodes, performing reasonably better that PVdF and comparable to the other functionalized polymers.
- LiAlg shows good ionic conductivity at 0.2 mS/cm, which is in the range as conventional SSEs. However, the LiAlg but forms LiOH on the contact surface with Li. This process is continuous and is detrimental to both the electrolyte conductivity and the interfacial resistance.
- The baseline conductivity of LAGP is observed to be at 0.5 mS/cm and the effect of prolonged Li contact is examined. It is observed that the reaction between Li and LAGP is chemical and electrochemical in nature and causes diminishing interfacial performance and more severely, causes the loss of mechanical integrity of the LAGP pellet.
- When used on the LAGP surface as a coating, the LiAlg prevents the direct contact between Li and LAGP. The combined electrolyte conductivity remains almost the same (0.4 mS/cm). However, the baseline interfacial performance of the pellet diminishes, possibly due to the brittle nature of the LiAlg coating causing poor mechanical contact. With prolonged exposure to Li, it was observed that the interfacial performance improves contrary to the observations from the bare pellet. This is possibly due to the LAGP inducing kinetic hindrances for water diffusion through the LiAlg layer - restricting the decomposition of LiAlg to a thin layer at the interface.

- For better understanding the scope of LiAlg as a secondary electrolyte, the test system needs to be simplified - this was done by replacing the LAGP with a LE. LiAlg was coated on different electrodes and cycled in different cycling windows to observe the ion conducting performance of the LiAlg. The results from these trials are extremely promising for the performance of LiAlg as a polymer electrolyte.

Thus, the experimental trials with LiAlg and LAGP reflect the immense potential of utilizing LiAlg as a secondary electrolyte and as a protective layer in solid state systems. These systems show stability against Li in addition to retaining good ionic conductivity. However, the brittleness of the LiAlg layer tends to induce poorer interfacial performance - this is linked back to specifically to the AlgA utilized. While the initial proof of concept is promising, there is scope for further optimizations to completely understand the advantages of the LiAlg in these systems.

5

Experimental work with Sodium Alginate

This chapter explains the results of the experiments carried out with NaAlg. Initially, the ionic conductivity of NaAlg is estimated, including the effect of water content and operating temperature. Then, the effect of pellet thickness on the interfacial resistance is studied. Subsequently, the ionic conductivity of NaAlg in Na systems is studied for its variation with water content. Due to the formation of NaOH on contact with Na, the testing configuration is changed to Na-aqueous electrodes. The variation of ionic conductivity with water content is studied again. Due to the shift to Na-aqueous electrode, the scope of NaAlg as aq. electrolytes and GPEs is studied due to higher conductivity and diminished interface resistances as compared to the solid NaAlg pellets. Finally, the cycling trials with the NaAlg electrolytes are explained and the observations are discussed.

5.1. Conductivity Measurements

5.1.1. Effect of water and operating temperature

Electrolytes with increasing water concentrations (ranging from a 2w% NaAlg solution upto a 100% NaAlg pellet) were prepared as mentioned earlier in Section 3.3. For ease of understanding, the mole fractions corresponding to the weight ratios are given in Table A.1. EIS measurements were then performed against blocking SS electrodes (refer appendix, Fig. A.20 to Fig. A.25) and the conductivity was measured at four different operating temperatures (20°C, 40°C, 60°C and 80°C). The conductivity comparison of the electrolytes at these different salt and water concentrations aids in studying the variation in the ionic conductivity which depends on the conflicting factors of charge carrier concentration and freedom of polymer chain motion which is directly influenced by the water concentration and operating temperature.

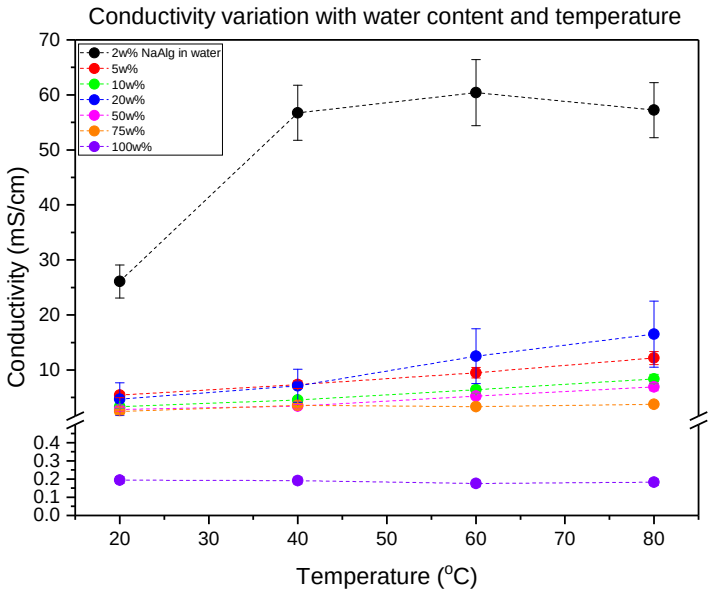

Figure 5.1: Variation of conductivity of NaAlg with varying water content and operating temperature

From Fig. 5.1, it can be observed that with increasing water content, for electrolytes with concentration ranging from 5w% NaAlg to 75w% NaAlg, there is an increase in conductivity with increasing temperature. This phenomenon is more pronounced at the higher water concentrations. As the salt concentration increases as in the case of the 100w% NaAlg pellet, the variation of conductivity with temperature is less pronounced. In the case of the 2w% NaAlg, the conductivity increases with increasing temperature till 60°C, but decreases slightly at 80°C. This phenomenon can be because at a certain temperature where the effect of concentration of ionic charge carriers (salt concentration) has an increase impact on the conductivity than the improved ionic mobility caused at the higher temperature. Fig. 5.2 gives a clearer comparison of the variation of conductivity with increasing water content at a constant temperature.

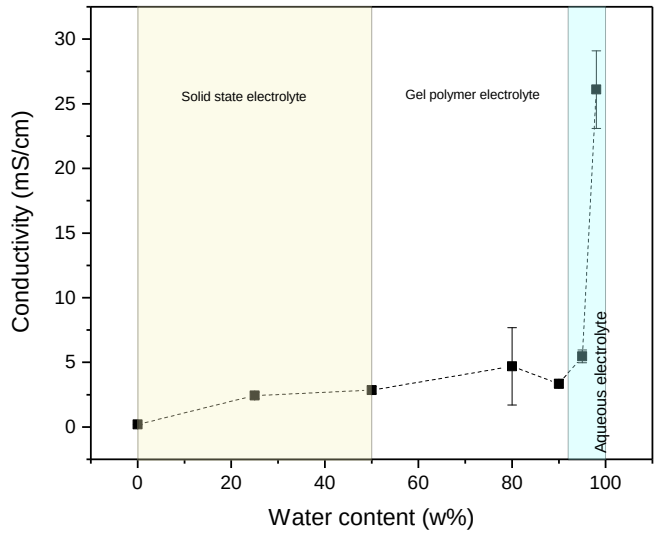

Figure 5.2: Variation of conductivity of NaAlg with varying water content at 20°C

At room temperature, the conductivity increases by a factor of 10 (from 0.2 to 2 mS/cm) when the water concentration increases from 0 to 20 w%. Between 25 w% and 90 w%, the conductivity improvement is only a factor of 1.5 (from 2 to 3 mS/cm) and between 90 w% and 98 w%, the conductivity improvement is by a factor of 9 (from 3 to 26 mS/cm). It is therefore evident that for increasing water content, conductivity remains within same margin between 25w% water to about 90w% of water - the effect of water concentration on the conductivity is

more pronounced at lower water concentrations and at very high concentrations. According to Wang et al. [47], the conduction mechanism in solvent-free solid polymer electrolytes is caused by the ion hopping along with the polymer chains vibrations. At low salt concentrations, higher water content relates to increase in freedom of movement thus causing the higher conductivity. With increasing salt content, the polymer chain vibrations are restricted causing the conductivity to reduce first but become constant within a range of salt concentrations. This is due to the stabilization of the conductivity caused due to conflict between increased charge carrier and diminished polymer vibrations. Further increasing the salt concentration will add more restriction to the polymer motion when finally, at very high salt concentration, the conduction mechanism is solely by virtue of solid-state ionic conduction.

5.1.2. Effect of pellet thickness

For analysing the solid state conduction mechanism of NaAlg, dry pellets (0% water) of different thickness but similar diameter were prepared and subjected to EIS. In electrolytes, the ionic conductivity is an intrinsic material characteristic while the interfacial resistance is caused due to mass transfer limitations along the electrode/electrolyte interface due to contact issues and also the ion conduction mechanisms through the particles in the bulk of the electrolyte (grain boundary diffusion). By varying the thickness and studying its corresponding effect on the interfacial resistance, it would shed more light into the ion conduction mechanism in solid NaAlg pellets. The results of the EIS are in agreement with the evidence of grain boundary diffusion, as can be seen in Fig. 5.3. All the pellets show similar ionic conductivity as expected (0.2mS/cm). As expected, with the increase in thickness and the subsequent increase in the concentrations of grains and grain boundaries, interfacial resistance too increases, (Table 5.1). This validates the solid state mechanism of conduction through NaAlg extending its scope as a viable solid-polymer electrolyte as well.

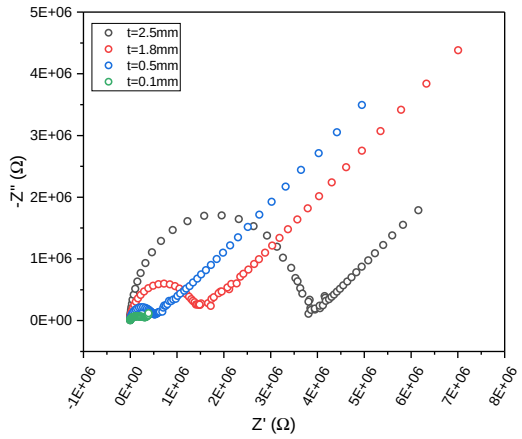

Figure 5.3: Variation of conductivity of NaAlg with varying pellet thickness at 20°C

Electrode system (with electrolyte thickness)	Interface Resistance (Ω)
SS/NaAlg/SS (0.1mm)	2.8E+05
SS/NaAlg/SS (0.533mm)	6.2E+05
SS/NaAlg/SS (1.82mm)	1.43E+06
SS/NaAlg/SS (2.5mm)	3.64E+06

Table 5.1: Interfacial resistance variation with thickness

5.1.3. Conductivity variations with water concentration in Na symmetrical configurations

After performing conductivity measurements with SS systems, the NaAlg pellets were subjected to similar EIS measurements against conductive Na systems. Since it is not possible to use higher water concentration against Na metal electrodes, these measurements were carried out with a 100% NaAlg, 90% NaAlg and 50w% NaAlg pellets (solid-polymer electrolyte configuration). Similar to earlier measurement, that there is an increase in conductivity of the NaAlg with increasing water content (from 0.1 to 1.5mS/cm) (refer appendix, Fig. A.28).

However, there was formation of white NaOH powder at the interface of the pellet and Na metal foil even in dried pellets, similar to the case of LiAlg (Section 4.2). The decomposition of the Na foil is continuous due to the perpetual diffusion of water molecules towards the interface. This formation of the NaOH layer is detrimental to the ion conduction at the electrode-electrolyte interface (refer appendix, Fig. A.29).

5.2. Experiments in Na aqueous systems

Due to the formation of NaOH at the interface of the pellets and Na foil, it was necessary to switch the cell testing configuration to a system which is not sensitive to water. The $Na_{0.44}MnO_2$ cathode (NMO) and the $NaTi_2(PO_4)_3$ anode (NaTP) were decided due the promising nature of their studies as Na aq. electrodes. The switch to the aqueous electrode systems would enable the utilization of higher water concentrations and would also eliminate the adverse effect of interfacial resistances.

5.2.1. Conductivity Measurements with Na aq. electrodes

Repeating the experiments preformed with the Na metal foil, pellets with 100%NaAlg, 85% NaAlg and 50% NaAlg were prepared and EIS measurements were carried out in a NMO/NaAlg/NaTP configuration with the new prepared Na aqueous electrodes (refer appendix, Fig. A.31). Similar to the earlier measurements, with increasing water content, the conductivity was observed to increase (from 0.1 to 1.5mS/cm) and the interfacial resistance decreases due to improved contact. No adverse reactions were observed at the interface, thus further experimentation were carried out with these electrodes.

5.3. Performance of NaAlg electrolytes (2w% aq. and GPE) in Na aqueous systems

Due to the switch to Na aq. electrodes, it was decided to switch testing for NaAlg solid polymer configurations to one with higher water concentrations due to increased ionic conductivities (from Section 5.1) - particularly a 2w% NaAlg aqueous solution and a 20w% NaAlg GPE. The NaAlg electrolytes were put under cycling trials and compared to a conventional Na aqueous electrolyte - 1M Na_2SO_4 in water to understand the performance of a typical aqueous system. The cell with the aq. electrolyte was prepared in a swagelok-type cell while the GPE was prepared in a solid state cell as explained in Section 3.3.

Fig. 5.4 compares the cycling curves for the three systems. It can be observed that the GPE and Na_2SO_4 systems show similar voltage cycling profiles, while in the case of the aqueous system, the slope of the discharge profile is comparatively shallow. Similarly, while comparing the charge and discharge capacities of both of the NaAlg configurations Fig. 5.5, it is clear that both of the systems show cycling behaviour during the charging cycle while displaying very low capacity during the discharge cycle. The Na_2SO_4 system on the other hand, undergoes high first cycle irreversible losses, and continues to provide low capacities with high coulombic efficiency.

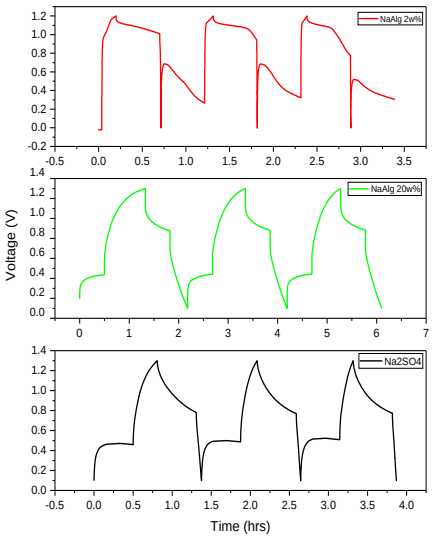

Figure 5.4: Cycling curves for the NaAlg electrolytes compared to the conventional electrolyte

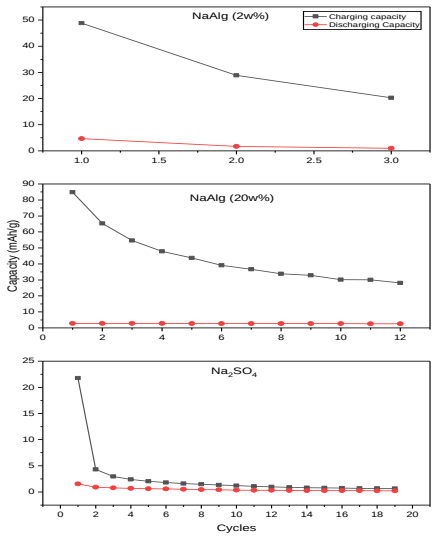

Figure 5.5: Capacity variation for the NaAlg electrolytes compared to the conventional electrolyte

To investigate further into the behaviour of the NaAlg cell, both the systems were disassembled and studied. In case of the aqueous system, it was observed that a black residue was formed in the separator containing the electrolyte - a sign of electrolyte degradation. Further information was observed when the cell with the NaAlg as GPE was disassembled. Fig. 5.6 and Fig. 5.7 show the formation of a black residue in the NaAlg aq. system and in the NaAlg GPE system, which gives more insight into the decomposition of the electrolyte. From is observed that in the NMO/electrolyte is isolated in the decomposition while the NaTP side remains pristine.

Figure 5.6: Electrolyte decomposition residue in NaAlg 2w% aq. system

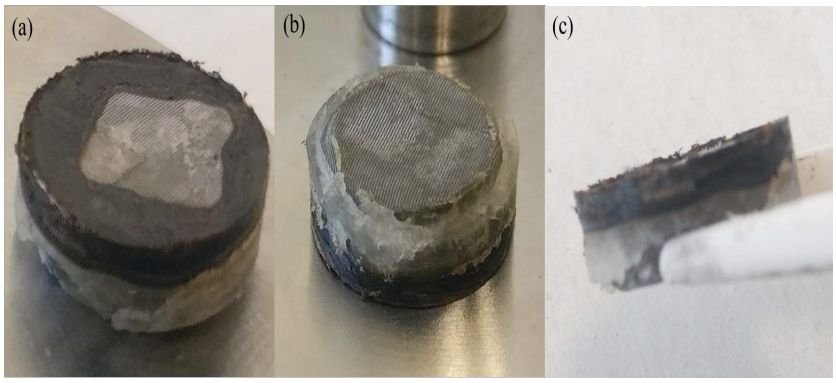

Figure 5.7: Electrolyte decomposition residue in NaAlg 20w% GPE system
(a)There is significant discolouration in the cathode side (NMO) of the cell.
(b) The anode side(NTP) remains more or less pristine.
(c) Contrast in colour along the cross section of the stack.

The isolation of the residue formation in the cathode/electrolyte interface coupled with the observations in capacity points to a parasitic redox reaction occurring at during de-sodiation of the cathode. The nature of this reaction is unknown, but XPS (X-ray photoelectron spectroscopy) of the interface would shed light on the decomposition. Additionally, using literature on Li-insertion chemistry, the decomposition mechanism could be theorised. Utilizing the work by Han et al. [48], Zhang et al. [49] and Wang et al. [50] on Lithium-rich metal oxide cathodes (xLi_2MnO_3-(1-x)$LiMO_2$ (M - Ni, Co, Mn, etc.), some possible reasons for the electrolyte decomposition may be drawn. The Na^+ extraction from the cathode could be causing the formation of active MnO_2 compound. The would cause the formation of an Mn redox couple. During de-sodiation, the formation and dissolution of Mn^{2+} ions into the aqueous electrolyte would induce cross-linking in the NaAlg chains, drastically reducing the ion conduction through the cathode/electrolyte interface and causing cell failure. Therefore, the decomposition and loss of cycling performance is possible due to the incompatibility between the cathode and the NaAlg. Hence, further system optimizations need to be done to understand the scope of NaAlg as electrolytes for Na systems.

5.4. Inferences from experimental trials with NaAlg

- The baseline ionic conductivity of NaAlg was calculated. The NaAlg show excellent conductivity at solid-state, gel polymer and aq. salt concentrations. The effect of temperature on the conductivity is more pronounced at higher water concentrations. In the GPE and solid state concentrations, the system is highly stable offering operating flexibility for these systems.
- The effect of thickness on the interfacial resistance of NaAlg pellets sheds light on the solid state-ion conduction mechanism inside the bulk of the electrolyte. This along with high ionic conductivity (0.2mS/cm comparable to other ceramic SSEs) also yields credibility for NaAlg to be utilized as solid-polymer electrolytes in addition to the aqueous and GPE configurations.
- Conductivity measurements of solid state NaAlg was done in Na system, which were found to be similar to measurements from the SS system. However, even dry NaAlg pellets react with the surface of Na metal forming NaOH, causing parasitic redox reactions at the electrode/electrolyte interface. Further optimizations needs to be done to isolate the optimal electrode configuration for using these NaAlg as solid state electrolytes. In this study, further testing was done with existing Na aqueous electrodes.

- Conductivity measurements for the solid state NaAlg pellets with the Na aqueous electrodes (NMO and NaTP) correspond with the earlier conductivity measurements in the Na system. Switching to aqueous electrode not only eliminates chemical degradation of NaAlg at the interface, but also allows the switch to testing with GPEs and aqueous concentrations (which experiments have shown to exhibit higher conductivity and reduced interfacial resistances)
- Cycling of 2w% NaAlg(aq.) electrolyte and 20w% NaAlg GPE display similar cycling profiles as compared to the conventional Na_2SO_4 aq. electrolyte. However, in case of the NaAlg systems, there is large variation in the charging and discharging capacities. Observations after disassembly show the formation of a black residue at the NMO/electrolyte interface. This is theorized to be due to the the dissolution of Mn^{2+} into the electrolyte causing cross-linking of the alginate chains at the interface. This is due to the electrochemical incompatibility of the cathode with the electrolyte. In the limited cycling, the charge capacity observed is promising, however system optimizations (different cathodes) need to be looked into to fully understand the scope of these materials as electrolytes for Na-aqueous batteries.

The experimental trials with NaAlg reveal the immense potential of NaAlg and their versatility as electrolytes - solid-state, gel polymer and aqueous. The effect of water concentration and temperature is established as well as the evidence of solid state ion conduction. However, further optimization of the test systems needs to be explores to realise the scope of NaAlg as electrolytes in Na batteries.

6

Conclusions and Recommendations

6.1. Conclusions

The goal of this thesis was to utilize NaAlg and LiAlg in improving solid-state batteries. To this extent and from the scope of Li systems, LiAlg was synthesized and was found to have excellent conductivity (0.2mS/cm) in solid-state concentration. LiAlg was then successfully used as a protective coating on an inorganic ceramic LAGP electrolyte to restrict the degradation caused by Li contact. The performance of LiAlg as a secondary electrolyte was also studied in different potential windows and the results showcase the immense potential of LiAlg as a solid state electrolyte.

In the scope of Na systems, the effect of water, operating temperature and pellet thickness on the ionic conductivity of the NaAlg proves its exceptional nature to behave as electrolytes in three different configurations - solid-state, gel polymer and aqueous liquid electrolytes. Due to the reaction of Na with the solid state NaAlg pellet, cycling trials were conducted adopting Na aqueous electrodes (NMO and NaTP) - utilizing the NaAlg in its aqueous and gel polymer configuration. Even though the cycling profiles of the two systems match with those of a standard electrolyte, both systems display performance in only the charging cycles. Observations of the systems reveal that a black residue is formed at the cathode/electrolyte interface - caused due to the Mn^{2+} induced cross-linking occurring at the interface during de-sodiation of the cathode. These observations point to the incompatibility of the cathode and the electrolyte and optimizations in the system need to be done to further investigate the performance of NaAlg as electrolytes. The conductivity experiments performed with NaAlg are extremely promising but further system optimizations need to be done to understand the scope of these materials are electrolytes for Na systems.

The study has thus established a proof of concept for the utilization of alginate salts in improving solid state Li-ion and Na-ion batteries.

6.2. Recommendations

During the course of the study, there were many points of intersection where the research scope could have taken any number of different paths. Some noteworthy paths that were left unexplored, if pursued, would be a great addition to further enhancing the scope of these alginate materials. Some of the prospective research scopes are mentioned below:

- Utilizing different alginic acid precursors for LiAlg and NaAlg preparation.

  Since there was significant difference in the visual characteristics of the commercial and synthesized NaAlg, utilizing alginic acid samples with different M/G ratios would ensure preparation of NaAlg and LiAlg with better gelation properties. This would assist in preparing better films, GPEs and solid-state pellets.

- Sandwiching LiAlg pellets on LAGP for better interfacial performance.

  LiAlg, if prepared with better AlgA precursors, would enable the preparation of solid-state pellets. These pellets could be used on the surface of LAGP pellets as a protective layer or even as a stand-alone solid electrolyte.

- Scope of LiAlg as aqueous electrolyte and GPE in Li aqueous systems would also serve as a viable alternative research path to move away from conventional organic electrolytes.

- Testing the LiAlg coating in electrodes which operate outside of the stable potential window of the organic electrolyte - this would expand the scope of LiAlg as stabilizing layer to prevent electrolyte decomposition at high voltages. Further, this would add more electrode-electrolyte combinations to be included in the scope of Li-ion research.

- Preparing an all-solid state battery by utilizing LiAlg in the electrode mixture [11] - this would be the next iterative step in solid-state batteries with LiAlg.

- Though the scope of LiAlg and NaAlg as binders has been investigated in detail, the studies have been limited to the anode system. Expanding the scope of the binders into cathode mixtures and understanding the electrochemical performance could be another potential avenue for sustainable batteries.

- In the NaAlg GPE cycled with Na aq. electrodes, the formation of the black residue on the cathode/electrolyte interface needs to be investigated. Using XPS techniques, decomposition compounds can be identified and traced to electrochemical phenomena. Performing cyclic voltammetry for NaAlg against these electrodes would shed light on the electrochemical decomposition mechanism. Further, preparing a solid-cell stack could shed some light on the water dependence of the degradation mechanism. The performance of the NaAlg electrolytes should also be characterized in various electrode combinations.

- Utilizing in-situ TEM analysis could help improve the understanding of the mechanism for Na^+ ion diffusion through NaAlg electrolytes.

A

Appendix

Various configurations for LiAlg and NaAlg

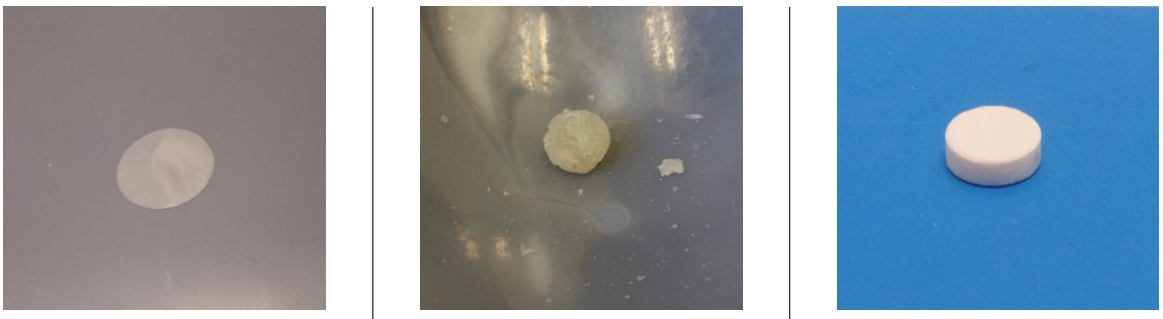

As free standing films | Gel polymer electrolyte | Solid polymer electrolyte

Figure A.1: Various configurations of the NaAlg testing

Figure A.2: Visual observation of LiAlg coated on Cu substrate - good adhesion to the Cu but brittle in nature

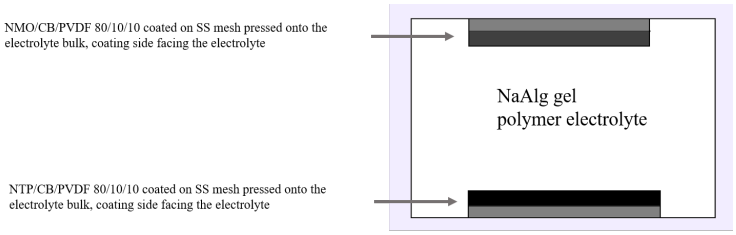

Figure A.3: Schematic representation of the NaAlg GPE testing/cycling configuration

EIS measurements for LiAlg and LAGP

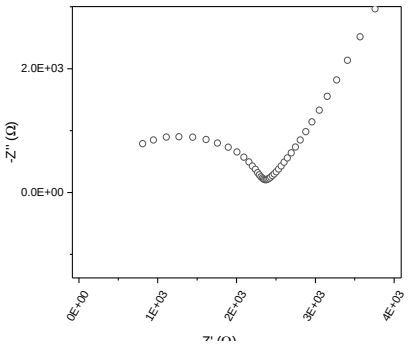

Figure A.4: EIS measurement for the LiAlg-soaked separator in SS symmetrical system

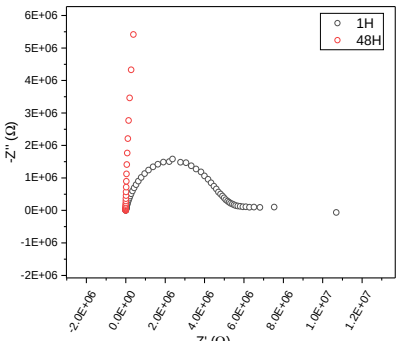

Figure A.5: EIS measurement for the LiAlg-soaked separator in Li symmetrical system - effect of prolonged Li contact

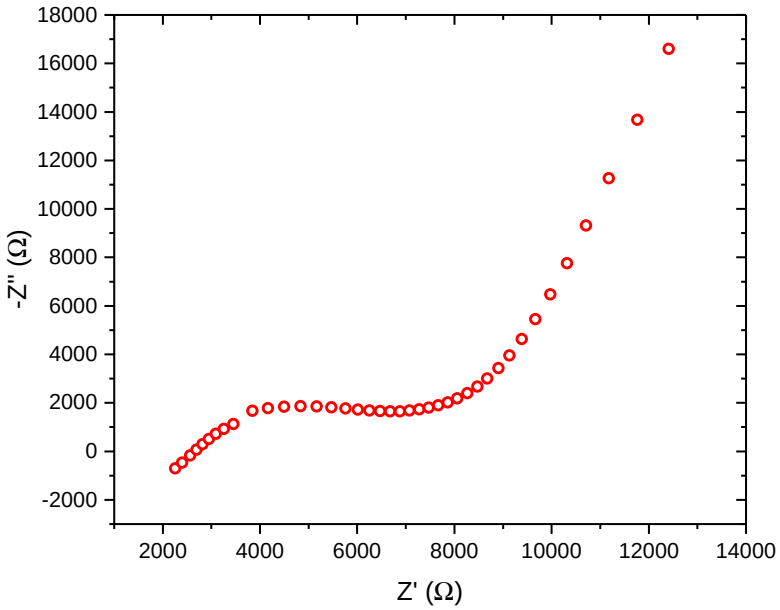

Figure A.6: EIS measurement for the bare LAGP pellet in SS symmetrical system

Cycling results for LiAlg coated electrodes

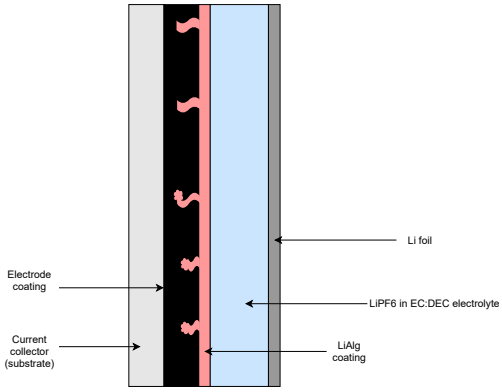

Figure A.7: Schematic representation of the LiAlg coated electrodes, where the LiAlg layer acts as a secondary electrode

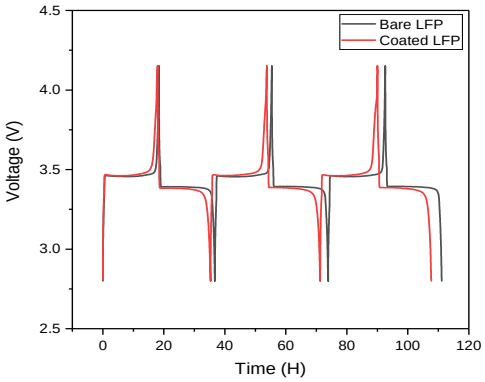

Figure A.8: Comparison of cycling curves at C/20 for the coated and bare LFP electrodes

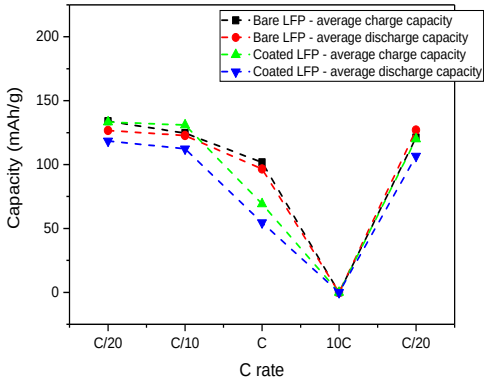

Figure A.9: Capacity variation with C rate for the coated and bare LFP electrodes

Performance comparison of the coated and bare LFP electrodes

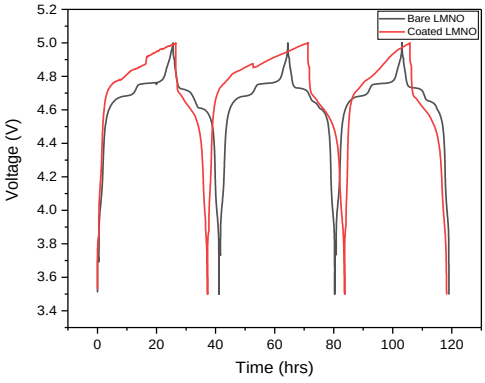

Figure A.10: Comparison of cycling curves at C/20 for the coated and bare LNMO electrodes

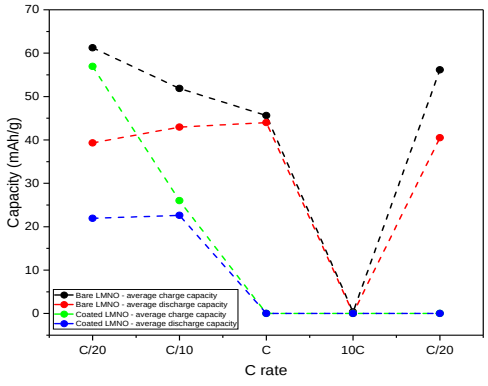

Figure A.11: Capacity variation with C rate for the coated and bare LNMO electrodes

Performance comparison of the coated and bare LNMO electrodes

The results from LMNO electrodes are interesting since these systems cycle upto 5V, which is on the edge of the stable potential window of the organic liquid electrolyte used in the cells. On cycling, it was observed that the uncoated LMNO electrode cycles as expected with decreasing capacity with increasing current densities (similar to the other cases). But in case of the coated electrode, the combined effects of the high cycling voltage and the high C rate, caused the cell to lose all cycling capacity and undergo cell failure. A reason for this would be the degradation of the electrolyte at the high voltages. But on the other hand, this could be caused due to the stresses induced at the high C rates which could cause mechanical failure in the LiAlg coating - caused due to the electrochemical degradation of the layer and subsequent contact loss.

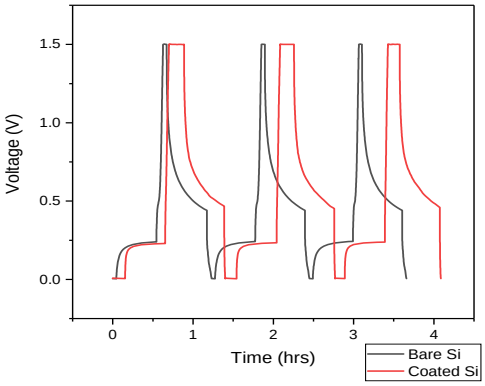

Figure A.12: Comparison of cycling curves at 1C for the coated and bare Si electrodes

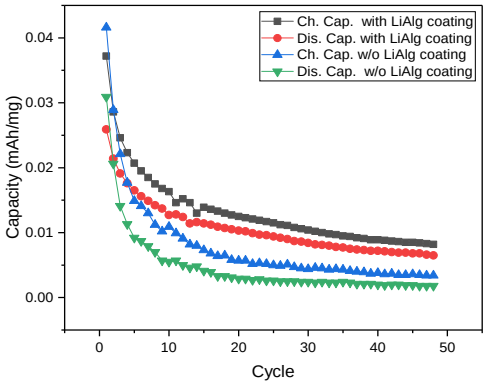

Figure A.13: Capacity variation for the coated and bare Si electrodes

Performance comparison of the coated and bare Si electrodes

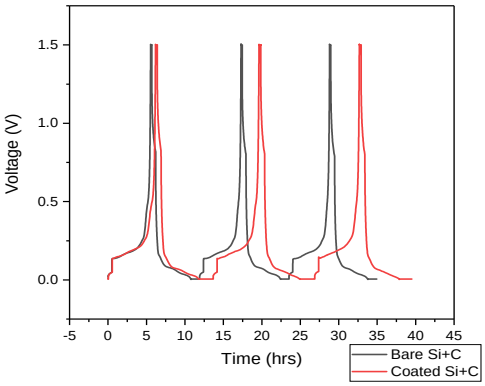

Figure A.14: Comparison of cycling curves at C/10 for the coated and bare Si/C composite electrodes

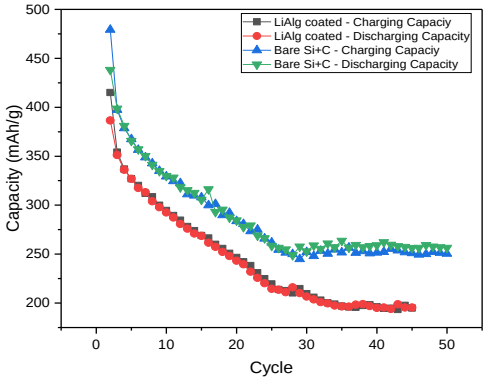

Figure A.15: Capacity variation for the coated and bare Si/C composite electrodes

Performance comparison of the coated and bare Si/C composite electrodes

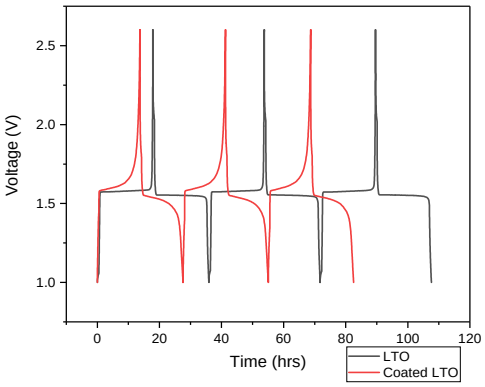

Figure A.16: Comparison of cycling curves at C/20 for the coated and bare LTO electrodes

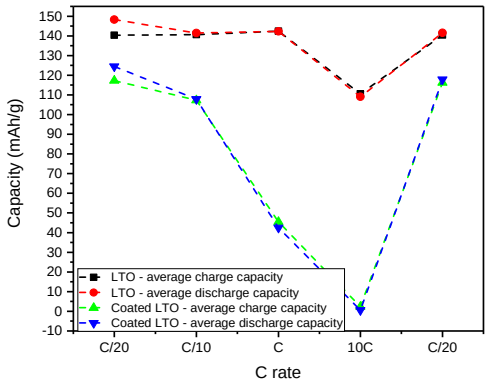

Figure A.17: Capacity variation for the coated and bare LTO electrodes

Performance comparison of the coated and bare LTO electrodes

EIS measurements for LiAlg coated electrodes

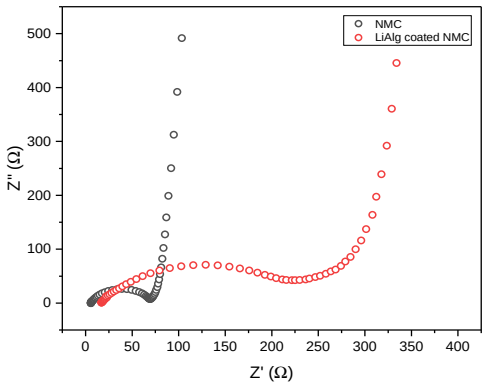

Figure A.18: EIS comparison between coated and bare NMC electrodes

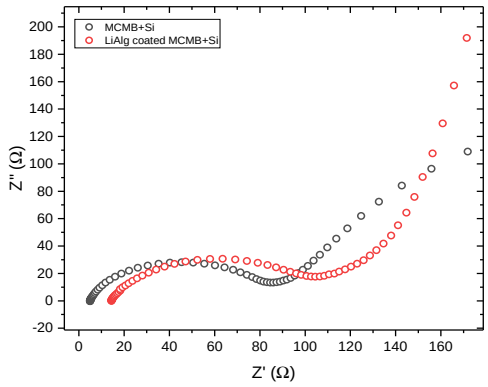

Figure A.19: EIS comparison between coated and bare Si/C composite electrodes

Raw EIS data for conductivity measurements of NaAlg - water and operating temperature dependent

Concentration	Mole Fraction	
Amount of NaAlg (w%)	M/G Residues	Water
2	1	1000
5	1	469
10	1	222
20	3	296
50	3	74
75	9	74
100	-	

Table A.1: Weight ratio to mole fraction equivalent - for different electrolyte concentrations

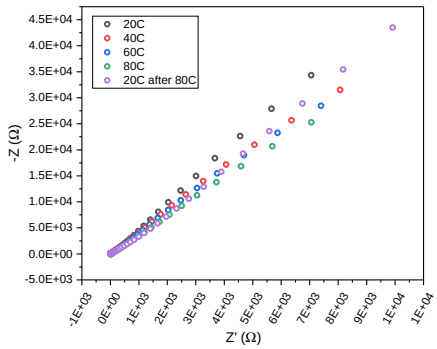

Figure A.20: EIS measurement for the 2w% NaAlg aq. electrolyte at different temperatures

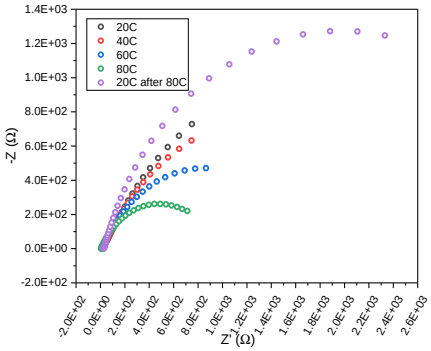

Figure A.21: EIS measurement for the 5w% NaAlg aq. electrolyte at different temperatures

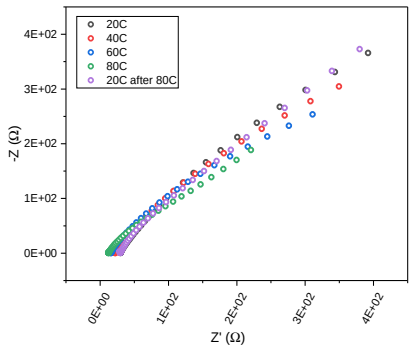

Figure A.22: EIS measurement for the 10w% NaAlg GPE at different temperatures

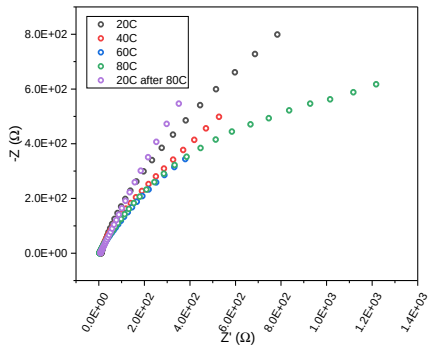

Figure A.23: EIS measurement for the 20w% NaAlg GPE at different temperatures

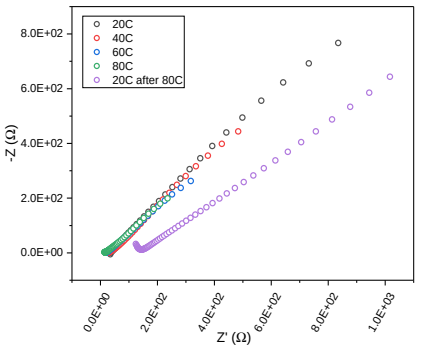

Figure A.24: EIS measurement for the 50w% NaAlg solid electrolyte at different temperatures

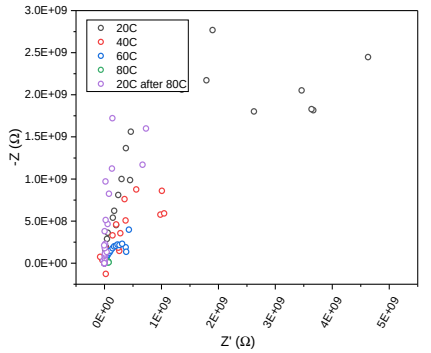

Figure A.25: EIS measurement for the 100w% NaAlg solid electrolyte at different temperatures

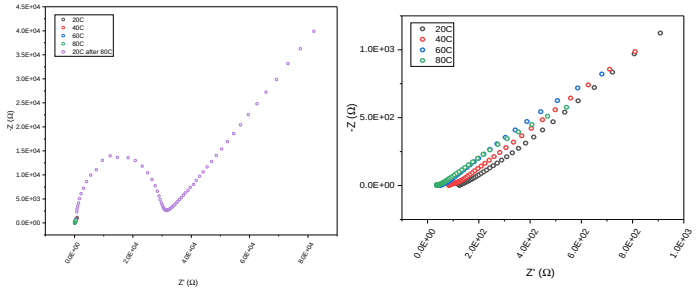

Figure A.26: EIS measurement for the 75w% NaAlg solid electrolyte at different temperatures

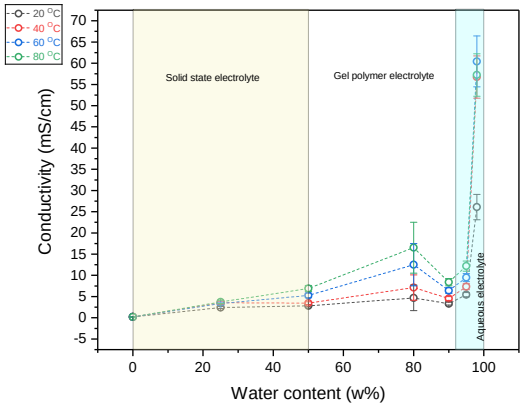

Figure A.27: Effect of operating temperature and water content on conductivity of NaAlg

Raw EIS data for conductivity measurements of NaAlg in Na symmetrical system

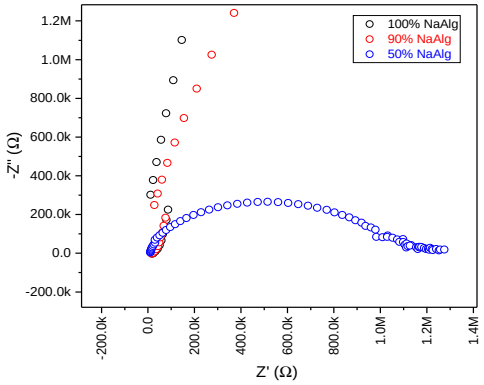

Figure A.28: EIS measurement for different solid state concentrations of NaAlg against Na symmetrical systems

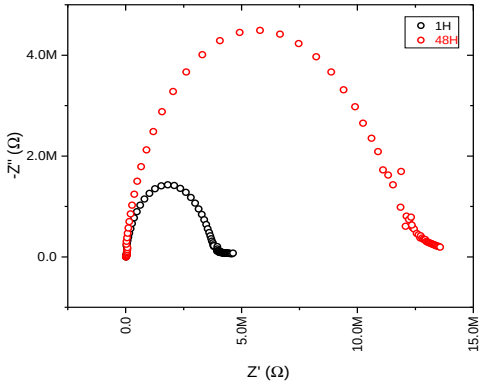

Figure A.29: Effect of soaking time on interfacial resistance of NaAlg

Application of LE at the interface of the NaAlg and Na

An additional experiment was carried out by applying a small quantity of sodium organic liquid electrolyte (1M (NaClO4) in EC:PC 1:1) at the interface of the dry pellet and Na foil. Even though the addition of the LE brings about an order or magnitude improvement in the interfacial resistance (Fig. A.30), on disassembling the cell,

the formation of NaOH was still present. Therefore, the testing configuration needed to be optimized for better understanding the electrochemical performance of the system.

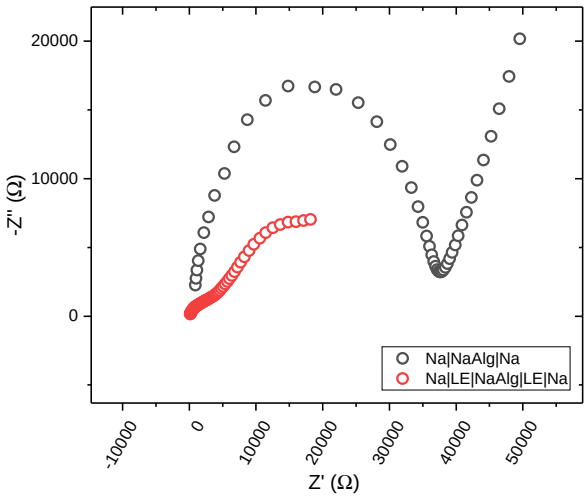

Figure A.30: Improvement in the interfacial resistance on application of LE on NaAlg pellet surface

EIS data for conductivity measurements of NaAlg in Na aqueous electrode system

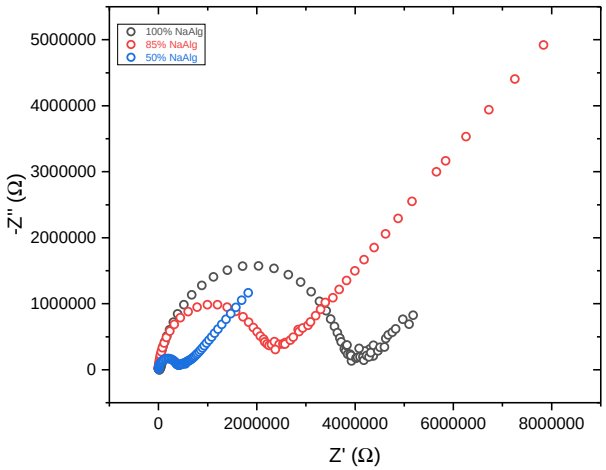

Figure A.31:]
EIS measurement for different solid state concentrations of NaAlg against Na aq. electrodes

Cycling trials with LAGP

In their study, Meesala et. al [11] reported promising cycling results in a Li/LAGP/LFP all-solid-state system. They prepared the cathode mixture utilizing LiTFSI as an additional component which along with the PVdF binder would form a secondary polymer electrolyte within the bulk of the cathode. However, the highly hygroscopic LiTFSI causes the assembly of this cell to require controlled environments of glove-boxes. LiAlg had already proven as an excellent secondary electrolyte in the LE system (and as a binder) and thus the following trials were conducted to the study the effect of LiAlg as the secondary electrolyte instead of LiTFSi would make the components air-stable during assembly. Various configurations were prepared to test the performance of LiAlg

in such scopes. However, many of these trials revealed no useful information. The following trials and their comparisons may shed some light on the performance of LiAlg in this scope.

- Cathode side testing
  - Li / LAGP / [LFP/CB/PVDF/LiTFSI]
  - Li / LAGP / [LFP/CB/PVDF/LiAlg]
- Anode side testing
  - Li / LAGP / [Si/CB/PVDF/LiTFSI]
  - Li / LAGP / [Si/CB/PVDF/LiAlg]

Cathode side testing

For the preparation of the half cells, electrode recipes were prepared with LFP as active material, CB as conductive additive, PVdF as the binder and LiTFSi or LiAlg powder as the additional component in a 10/2/1/7 ratio [11]. The powders were mixed with the NMP solvent, to form the electrode slurry. The slurry was subsequently coated onto an LAGP pellet and dried. The pellet was finally prepared into a half cell against Li foil and cycled between 2.8 - 4.15 V. Identical half cells were prepared with LiAlg and LiTFSi. Fig. A.32 shows the cycling curves for both the cells. It is evident from the comparison that while the LiTFSi cell performs well, the LiAlg cell show minor charge capacity, but no discharge capacity.

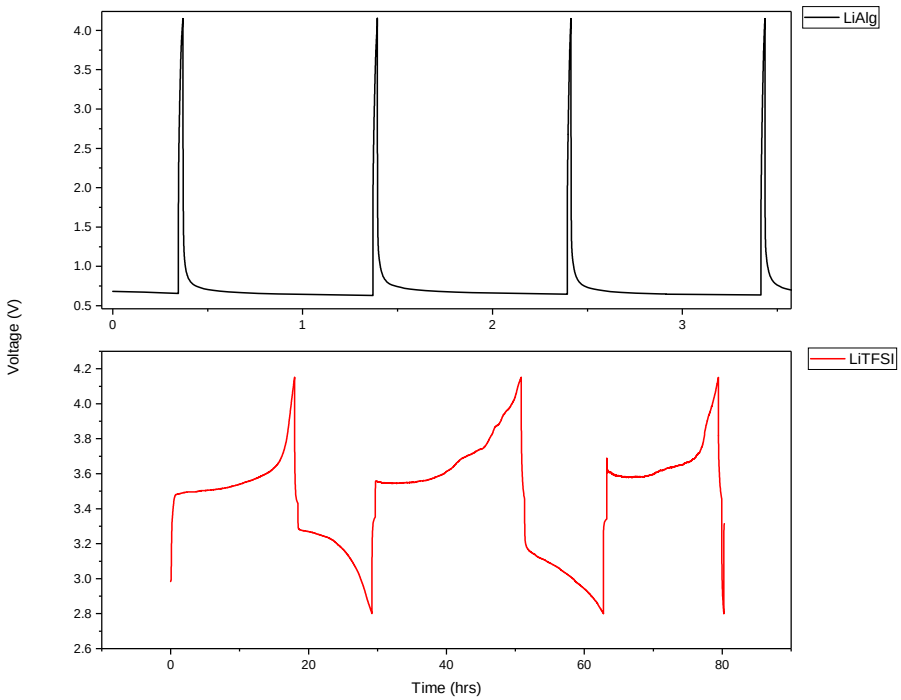

Figure A.32: Comparison of cycling curves for the LAGP half cells with additives in the cathode

Anode side testing

Similar cells were prepared on the anode side, replacing the LFP with Si powder as the active material and cycled between 5 mV and 1.5 V. Fig. A.33 shows the cycling curves for both the cells. In contrary to the LFP cells, the LiAlg cell performs well, while the LiTFSI system cell does not display any performance.

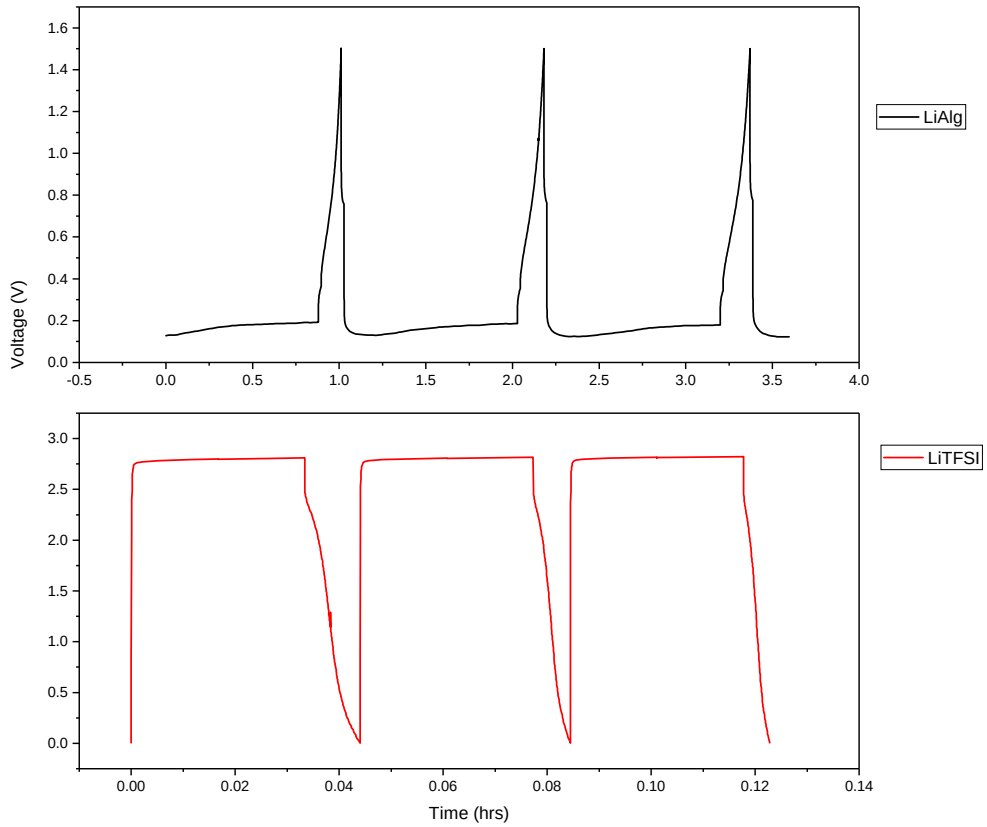

Figure A.33: Comparison of cycling curves for the LAGP half cells with additives in the anode

The LiTFSI and PVdF mixture combine to form a GPE with interspersed Li^+ ions in the electrolyte bulk. The preparation of such a GPE in the cathode would allow greater ionic conduction through the electrode bulk. LiAlg on the other hand, has been tested to perform as a GPE though the Li^+ ions are coordinated with the alginate polymer chain. The poor performance of the LiAlg at the cathode could be theorized as due to negative interactions caused inside the electrode bulk. LiAlg could be having an adverse effect on the de-lithiation of the cathode, possibly due to the interactions between the exiting Li^+ and the polymer chains. This is in contrast with the anode side results, where the LiAlg shows better performance compared to the LiTFSI. This could be due to the Li^+ ions in the LiTFSi/PVdF GPE causing in-situ Li mobility within the anode bulk. The LiAlg on the other hand, due to the polymer coordination of the Li^+, does not cause this phenomenon. Further testing needs to be done to accurately pin-point the mechanisms in both these systems. As such, it would be interesting to combine the two half cells to prepare an all-solid-state cell and explore the feasibility of the system.

Bibliography

[1] IPCC Climate Change et al. Mitigation of climate change. *Contribution of Working Group III to the Fifth Assessment Report of the Intergovernmental Panel on Climate Change*, 1454, 2014.

[2] M Stanley Whittingham. Electrical energy storage and intercalation chemistry. *Science*, 192(4244): 1126–1127, 1976.

[3] Naoki Nitta, Feixiang Wu, Jung Tae Lee, and Gleb Yushin. Li-ion battery materials: present and future. *Materials today*, 18(5):252–264, 2015.

[4] XiaoLong Xu, SiXu Deng, Hao Wang, JingBing Liu, and Hui Yan. Research progress in improving the cycling stability of high-voltage lini 0.5 mn 1.5 o 4 cathode in lithium-ion battery. *Nano-micro letters*, 9(2): 22, 2017.

[5] Huajun Tian, Fengxia Xin, Xiaoliang Wang, Wei He, and Weiqiang Han. High capacity group-IV elements (Si, Ge, Sn) based anodes for lithium-ion batteries. *Journal of Materiomics*, 1(3):153–169, 2015.

[6] Rachel DeWees and Hui Wang. Synthesis and properties of nasicon-type latp and lagp solid electrolytes. *ChemSusChem*, 2019.

[7] Theodosios Famprikis, Pieremanuele Canepa, James A. Dawson, M. Saiful Islam, and Christian Masquelier. Fundamentals of inorganic solid-state electrolytes for batteries. *Nature Materials*, pages 1–14, 08 2019. doi: 10.1038/s41563-019-0431-3.

[8] Verónica Palomares, Paula Serras, Irune Villaluenga, Karina B. Hueso, Javier Carretero-González, and Teófilo Rojo. Na-ion batteries, recent advances and present challenges to become low cost energy storage systems. *Energy Environ. Sci.*, 5:5884–5901, 2012. doi: 10.1039/C2EE02781J. URL http://dx.doi.org/10.1039/C2EE02781J.

[9] Changhong Wang, Qian Sun, Yulong Liu, Yang Zhao, Xia Li, Xiaoting Lin, Mohammad Norouzi Banis, Minsi Li, Weihan Li, Keegan R Adair, et al. Boosting the performance of lithium batteries with solid-liquid hybrid electrolytes: Interfacial properties and effects of liquid electrolytes. *Nano Energy*, 48:35–43, 2018.

[10] Qipeng Yu, Da Han, Qingwen Lu, Yan-Bing He, Song Li, Qi Liu, Cuiping Han, Feiyu Kang, and Baohua Li. Constructing Effective Interfaces for $Li_{1.5}Al_{0.5}Ge_{1.5}PO4_3$ Pellets To Achieve Room-Temperature Hybrid Solid-State Lithium Metal Batteries. *ACS applied materials & interfaces*, 11(10):9911–9918, 2019.

[11] Yedukondalu Meesala, Chen-Yu Chen, Anirudha Jena, Yu-Kai Liao, Shu-Fen Hu, Ho Chang, and Ru-Shi Liu. All-Solid-State Li-Ion Battery Using $Li_{1.5}Al_{0.5}Ge_{1.5}PO4_3$ As Electrolyte Without Polymer Interfacial Adhesion. *The Journal of Physical Chemistry C*, 122(26):14383–14389, 2018.

[12] Igor Kovalenko, Bogdan Zdyrko, Alexandre Magasinski, Benjamin Hertzberg, Zoran Milicev, Ruslan Burtovyy, Igor Luzinov, and Gleb Yushin. A major constituent of brown algae for use in high-capacity li-ion batteries. *Science*, 334(6052):75–79, 2011.

[13] J-S Bridel, Thierry Azais, Mathieu Morcrette, J-M Tarascon, and Dominique Larcher. Key parameters governing the reversibility of si/carbon/cmc electrodes for li-ion batteries. *Chemistry of materials*, 22(3): 1229–1241, 2009.

[14] Delphine Guy, Bernard Lestriez, and Dominique Guyomard. New composite electrode architecture and improved battery performance from the smart use of polymers and their properties. *Advanced Materials*, 16 (6):553–557, 2004.

[15] Dominic Bresser, Daniel Buchholz, Arianna Moretti, Alberto Varzi, and Stefano Passerini. Alternative binders for sustainable electrochemical energy storage–the transition to aqueous electrode processing and bio-derived polymers. *Energy & Environmental Science*, 11(11):3096–3127, 2018.

[16] Alexandre Magasinski, Bogdan Zdyrko, Igor Kovalenko, Benjamin Hertzberg, Ruslan Burtovyy, Christopher F Huebner, Thomas F Fuller, Igor Luzinov, and Gleb Yushin. Toward efficient binders for li-ion battery si-based anodes: polyacrylic acid. *ACS applied materials & interfaces*, 2(11):3004–3010, 2010.

[17] Hilmi Buqa, Michael Holzapfel, Frank Krumeich, Claudia Veit, and Petr Novák. Study of styrene butadiene rubber and sodium methyl cellulose as binder for negative electrodes in lithium-ion batteries. *Journal of Power Sources*, 161(1):617–622, 2006.

[18] Jin-Hyon Lee, Sangkyu Lee, Ungyu Paik, and Young-Min Choi. Aqueous processing of natural graphite particulates for lithium-ion battery anodes and their electrochemical performance. *Journal of power sources*, 147(1-2):249–255, 2005.

[19] Jin-Hyon Lee, Ungyu Paik, Vincent A Hackley, and Young-Min Choi. Effect of poly (acrylic acid) on adhesion strength and electrochemical performance of natural graphite negative electrode for lithium-ion batteries. *Journal of Power Sources*, 161(1):612–616, 2006.

[20] Nikolaus S Hochgatterer, Mario R Schweiger, Stefan Koller, Peter R Raimann, Thomas Wöhrle, Calin Wurm, and Martin Winter. Silicon/graphite composite electrodes for high-capacity anodes: influence of binder chemistry on cycling stability. *Electrochemical and solid-state letters*, 11(5):A76–A80, 2008.

[21] Nuria Cuesta, Alberto Ramos, Ignacio Cameán, Cristina Antuña, and Ana B García. Hydrocolloids as binders for graphite anodes of lithium-ion batteries. *Electrochimica Acta*, 155:140–147, 2015.

[22] You Kyeong Jeong, Tae-woo Kwon, Inhwa Lee, Taek-Soo Kim, Ali Coskun, and Jang Wook Choi. Millipede-inspired structural design principle for high performance polysaccharide binders in silicon anodes. *Energy & Environmental Science*, 8(4):1224–1230, 2015.

[23] Alberto García, Mario Culebras, Maurice N Collins, and James J Leahy. Stability and rheological study of sodium carboxymethyl cellulose and alginate suspensions as binders for lithium ion batteries. *Journal of Applied Polymer Science*, 135(17):46217, 2018.

[24] Gert Berckmans, Maarten Messagie, Jelle Smekens, Noshin Omar, Lieselot Vanhaverbeke, and Joeri Van Mierlo. Cost projection of state of the art lithium-ion batteries for electric vehicles up to 2030. *Energies*, 10(9):1314, 2017.

[25] David L Wood III, Jianlin Li, and Claus Daniel. Prospects for reducing the processing cost of lithium ion batteries. *Journal of Power Sources*, 275:234–242, 2015.

[26] S Mohanapriya, S.D. Bhat, AK Sahu, A Manokaran, R Vijayakumar, S Pitchumani, P Sridhar, and AK Shukla. Sodium alginate based proton-exchange membranes as electrolytes for DMFCs. *Energy & Environmental Science*, 3(11):1746–1756, 2010.

[27] Y. O. Iwaki, M Hernandez Escalona, J.R. Briones, and A Pawlicka. Sodium alginate based ionic conducting membranes. *Molecular Crystals and Liquid Crystals*, 554(1):221–231, 2012.

[28] Masaki Yamagata, Kazunari Soeda, Shigeaki Yamazaki, and Masashi Ishikawa. Alginate gel containing an ionic liquid and its application to non-aqueous electric double layer capacitors. *Electrochemical and Solid-State Letters*, 14(11):A165–A169, 2011.

[29] Alginic acid - Polymannuronic acid - A17582 - Alfa Aesar. https://www.alfa.com/en/catalog/A17582/. (Accessed on 09/14/2019).

[30] Sodium Hydroxide, BioXtra, ≥98%, pellets (anhydrous) | NaOH | Sigma-Aldrich. https://www.sigmaaldrich.com/catalog/product/sigald/s8045?lang=en&region=NL. (Accessed on 09/19/2019).

[31] Lithium Hydroxide Monohydrate, ACS reagent, ≥98.0% | LiOH | Sigma-Aldrich. https://www.sigmaaldrich.com/catalog/product/sigald/402974?lang=en&region=NL, . (Accessed on 09/19/2019).

[32] Alginic acid - Sodium salt, high viscosity - Sodium alginate - J61887 - Alfa Aesar. https://www.alfa.com/en/catalog/J61887/. (Accessed on 09/14/2019).

[33] Mohamed Fertah, Ahmed Belfkira, Moha Taourirte, François Brouillette, et al. Extraction and characterization of sodium alginate from moroccan laminaria digitata brown seaweed. *Arabian Journal of Chemistry*, 10:S3707–S3714, 2017.

[34] Ivan Donati, Amedeo Vetere, Amelia Gamini, Gudmund Skjåk-Bræk, Anna Coslovi, Cristiana Campa, and Sergio Paoletti. Galactose-substituted alginate: preliminary characterization and study of gelling properties. *Biomacromolecules*, 4(3):624–631, 2003.

[35] A Penman and G.R. Sanderson. A method for the determination of uronic acid sequence in alginates. *Carbohydrate Research*, 25(2):273–282, 1972.

[36] Huisuo Huang, Ingolf U. Grün, Mark R. Ellersieck, and A. D. Clarke. Measurement of total sodium alginate in restructured fish products using fourier transform infrared spectroscopy. *EC Nutrition*, 2017.

[37] Lithium Carbonate, puriss. p.a., ACS reagent, reagent (for microscopy), ≥99.0% (T) | Li2CO3 | Sigma-Aldrich. https://www.sigmaaldrich.com/catalog/product/sigald/62470?lang=en&region=NL, . (Accessed on 09/19/2019).

[38] Germanium(IV) Oxide ≥99.99% trace metals basis | Sigma-Aldrich. https://www.sigmaaldrich.com/catalog/product/aldrich/483702?lang=en&region=NL. (Accessed on 09/19/2019).

[39] Aluminum Oxide 99.997% trace metals basis | Sigma-Aldrich. https://www.sigmaaldrich.com/catalog/product/aldrich/202606?lang=en&region=NL. (Accessed on 09/19/2019).

[40] Ammonium dihydrogenphosphate 99.999% trace metals basis | Sigma-Aldrich. https://www.sigmaaldrich.com/catalog/product/aldrich/204005?lang=en&region=NL. (Accessed on 09/19/2019).

[41] X-ray Powder Diffraction (XRD). https://serc.carleton.edu/research_education/geochemsheets/techniques/XRD.html. (Accessed on 09/11/2019).

[42] Ampcera Solid Electrolyte, LAGP, $Li_{1.5}Al_{0.5}Ge_{1.5}P_3O_{12}$ Powder – MSE Supplies LLC. https://www.msesupplies.com/products/li1-5al0-5ge1-5p3o12-lagp-powder-solid-state-electrolyte-for-advanced-lithium-batteries?variant=32297221892. (Accessed on 09/11/2019).

[43] Joykumar S Thokchom, Nutan Gupta, and Binod Kumar. Superionic conductivity in a lithium aluminum germanium phosphate glass–ceramic. *Journal of the Electrochemical Society*, 155(12):A915–A920, 2008.

[44] B Kumar, D Thomas, and Jitendra Kumar. Space-charge-mediated superionic transport in lithium ion conducting glass–ceramics. *Journal of The Electrochemical Society*, 156(7):A506–A513, 2009.

[45] Elahe Talaie, Patrick Bonnick, Xiaoqi Sun, Quan Pang, Xiao Liang, and Linda F Nazar. Methods and protocols for electrochemical energy storage materials research. *Chemistry of Materials*, 29(1):90–105, 2016.

[46] Jared Tippens, John Miers, Arman Afshar, John Lewis, Francisco Javier Quintero Cortes, Haipeng Qiao, Thomas S Marchese, Claudio V Di Leo, Christopher Saldana, and Matthew T McDowell. Visualizing Chemo-Mechanical Degradation of a Solid-State Battery Electrolyte. *ACS Energy Letters*, 2019.

[47] Yumei Wang, Shufeng Song, Chaohe Xu, Ning Hu, Janina Molenda, and Li Lu. Development of solid-state electrolytes for sodium-ion battery - a short review. *Nano Materials Science*, 2019.

[48] Zenghui Han, Hui Zhan, and Yunhong Zhou. Preparation and performance of layered li $Li_{0.182}Ni_{0.182}Co_{0.091}Mn_{0.545}O_2$ cathode with different binders. *Materials Letters*, 114:48–51, 2014.

[49] Shao-Jian Zhang, Ya-Ping Deng, Qi-Hui Wu, Yao Zhou, Jun-Tao Li, Zhan-Yu Wu, Zu-Wei Yin, Yan-Qiu Lu, Chong-Heng Shen, Ling Huang, et al. Sodium-alginate-based binders for lithium-rich cathode materials in lithium-ion batteries to suppress voltage and capacity fading. *ChemElectroChem*, 5(9):1321–1329, 2018.

[50] Zhiyuan Wang, Shaohua Luo, Jie Ren, Dan Wang, and Xiwei Qi. Enhanced electrochemical performance of li-rich cathode $Li[Li_{0.2}Mn_{0.54}Ni_{0.13}Co_{0.13}O_2]$ by surface modification with lithium ion conductor Li_3PO_4. *Applied Surface Science*, 370:437–444, 2016.